



**HAL**  
open science

## ENSO climate forcing of the marine mercury cycle in the Peruvian Upwelling Zone Does Not Affect Methylmercury Levels of Marine Avian Top Predators

Marina Renedo, David Point, Jeroen E. Sonke, Anne Lorrain, Hervé Demarcq, Michelle Graco, Daniel Grados, Dimitri Gutiérrez, Anaïs Médieu, Jean Marie Munaron, et al.

### ► To cite this version:

Marina Renedo, David Point, Jeroen E. Sonke, Anne Lorrain, Hervé Demarcq, et al.. ENSO climate forcing of the marine mercury cycle in the Peruvian Upwelling Zone Does Not Affect Methylmercury Levels of Marine Avian Top Predators. *Environmental Science and Technology*, 2021, 55 (23), pp.15754-15765. 10.1021/acs.est.1c03861 . hal-03566681

**HAL Id: hal-03566681**

**<https://hal.umontpellier.fr/hal-03566681v1>**

Submitted on 20 Apr 2023

**HAL** is a multi-disciplinary open access archive for the deposit and dissemination of scientific research documents, whether they are published or not. The documents may come from teaching and research institutions in France or abroad, or from public or private research centers.

L'archive ouverte pluridisciplinaire **HAL**, est destinée au dépôt et à la diffusion de documents scientifiques de niveau recherche, publiés ou non, émanant des établissements d'enseignement et de recherche français ou étrangers, des laboratoires publics ou privés.

## ENSO Climate Forcing of the Marine Mercury Cycle in the Peruvian Upwelling Zone Does Not Affect Methylmercury Levels of Marine Avian Top Predators

Renedo Marina <sup>1,\*</sup>, Point David <sup>1,\*</sup>, Sonke Jeroen E. <sup>1</sup>, Lorrain Anne <sup>2</sup>, Demarcq Herve <sup>3</sup>, Graco Michelle <sup>4</sup>, Grados Daniel <sup>4</sup>, Gutiérrez Dimitri <sup>4</sup>, Médiéu Anais <sup>2</sup>, Munaron Jean-Marie <sup>2</sup>, Pietri Alice <sup>4</sup>, Colas François <sup>5</sup>, Tremblay Yann <sup>3</sup>, Roy Amedee <sup>3</sup>, Bertrand Arnaud <sup>3</sup>, Lanco Bertrand Sophie <sup>3</sup>

<sup>1</sup> Géosciences Environnement Toulouse (GET)-Institut de Recherche pour le Développement (IRD), CNRS, Université de Toulouse, 14 Avenue Edouard Belin, Toulouse 31400, France

<sup>2</sup> Univ Brest, CNRS, IRD, Ifremer, LEMAR, Plouzané F-29280, France

<sup>3</sup> IRD, MARBEC (Univ. Montpellier, CNRS, Ifremer, IRD), Sète 34203, France

<sup>4</sup> Instituto del Mar del Perú (IMARPE), LOCEAN IPSL (IRD/CNRS/SU/MNHN)Esquina Gamarra y General Valle, Callao 07021, Peru

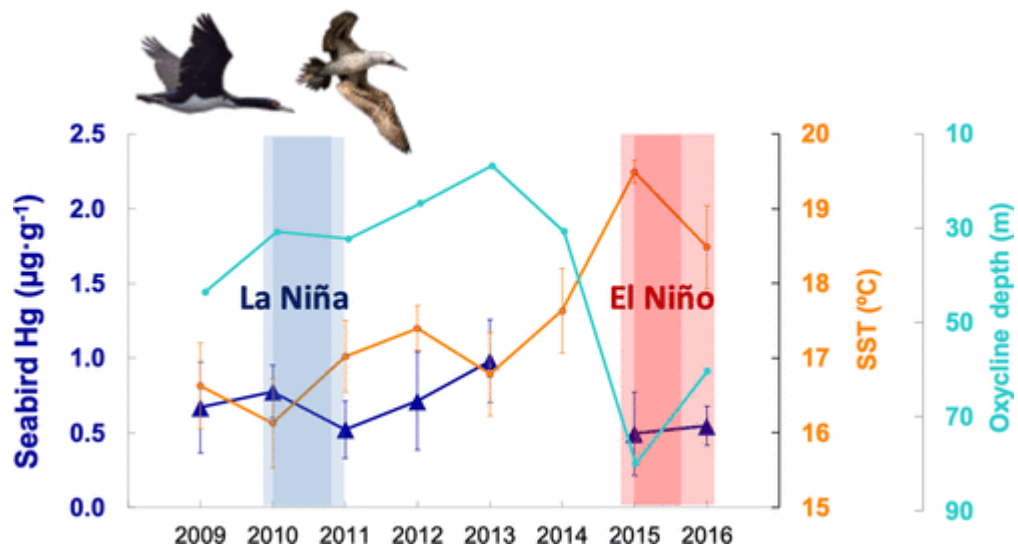
<sup>5</sup> LOCEAN IPSL (IRD/CNRS/SU/MNHN), 4 Place Jussieu, Paris 75252, France

\* Corresponding authors : Marina Renedo, email address : [mrenedoelizalde@gmail.com](mailto:mrenedoelizalde@gmail.com) ; David Point, email address : [david.point@ird.fr](mailto:david.point@ird.fr)

### Abstract :

Climate change is expected to affect marine mercury (Hg) biogeochemistry and biomagnification. Recent modeling work suggested that ocean warming increases methylmercury (MeHg) levels in fish. Here, we studied the influence of El Niño Southern Oscillations (ENSO) on Hg concentrations and stable isotopes in time series of seabird blood from the Peruvian upwelling and oxygen minimum zone. Between 2009 and 2016, La Niña (2011) and El Niño conditions (2015–2016) were accompanied by sea surface temperature anomalies up to 3 °C, oxycline depth change (20–100 m), and strong primary production gradients. Seabird Hg levels were stable and did not co-vary significantly with oceanographic parameters, nor with anchovy biomass, the primary dietary source to seabirds (90%). In contrast, seabird  $\Delta^{199}\text{Hg}$ , proxy for marine photochemical MeHg breakdown, and  $\delta^{15}\text{N}$  showed strong interannual variability (up to 0.8 and 3‰, respectively) and sharply decreased during El Niño. We suggest that lower  $\Delta^{199}\text{Hg}$  during El Niño represents reduced MeHg photodegradation due to the deepening of the oxycline. This process was balanced by equally reduced Hg methylation due to reduced productivity, carbon export, and remineralization. The non-dependence of seabird MeHg levels on strong ENSO variability suggests that marine predator MeHg levels may not be as sensitive to climate change as is currently thought.

## Graphical abstract



**Keywords :** Hg stable isotopes, MIF, Northern Humboldt current system, climate change, ecology

## 62 **1 Introduction**

63 Mercury (Hg) is a pollutant of major concern, efficiently bioassimilated and bioaccumulated in  
64 its methylmercury form (MeHg). It poses risks for the health of marine top predators, and  
65 humans who are mainly exposed to MeHg via seafood consumption <sup>1</sup>. In the industrial era,  
66 anthropogenic Hg emissions have exceeded natural volcanic and soil degassing emissions by a  
67 factor of seven <sup>2</sup>, resulting in similar enrichment of atmospheric and surface ocean Hg levels  
68 <sup>2,3</sup>. The biogeochemical Hg cycle is highly complex and comprises multiple chemical and  
69 biological transformations that control marine MeHg formation, breakdown and bioavailability  
70 to marine organisms, such as methylation/demethylation, redox reactions or photochemical  
71 processes. Mercury methylation is thought to be mainly driven by anaerobic micro-organisms  
72 within the water column, with a peak in net MeHg production at depth, in oceanic oxygen  
73 minimum zones (OMZ) <sup>4-6</sup> where organic matter remineralisation rates are the highest.  
74 Consequently, the depth of occurrence of pelagic fish has been identified as a prominent control  
75 factor on MeHg concentrations in marine predators <sup>7</sup>.

76 The impact of climate change forcing on the net production of marine MeHg represents  
77 a yet unknown and critical focal point of Hg research <sup>8-10</sup>. Global estimations predict rising  
78 seawater temperatures of 1.1 to 2°C by 2100 depending on emission scenarios <sup>11</sup>, an enhanced  
79 level of ocean acidification and oxygen loss <sup>12</sup>, reduced ocean primary production <sup>13</sup> and the  
80 expansion of OMZ <sup>14,15</sup>. Global warming is also expected to cause the loss of coastal resources  
81 and reduce the productivity of fisheries and aquaculture, with fisheries models estimating a  
82 decrease of 1.5 to 3.4 million tons of annual global marine fisheries catches during the 21<sup>st</sup>  
83 century <sup>16,17</sup>. These changes in oceanographic dynamics, primary production, OMZ extension  
84 and ocean-atmosphere exchanges can potentially influence marine MeHg production,  
85 bioavailability and transfer in the food web <sup>8,10,18</sup>. Experimental studies on estuarine and  
86 freshwater fish showed that rising water temperatures could increase MeHg bioaccumulation

87 levels <sup>19,20</sup>. A recent modelling study also predicted increasing trends of MeHg concentrations  
88 in fish from the Gulf of Maine due to warmer seawater temperatures <sup>9</sup>. The authors also  
89 suggested that overfishing could lead to enhanced MeHg accumulation in some marine fish  
90 species due to subsequent dietary shifts <sup>9</sup>. However, modelling studies present limitations  
91 relative to the most probable warming scenarios, and the complex connections between  
92 biogeochemical and ecological processes operating at regional and global scales. Experimental  
93 studies and long-term observations in relevant warming marine ecosystems are needed to help  
94 capture the complexity and coupling between baseline and trophic processes that govern MeHg  
95 concentrations in the food web.

96         The Northern Humboldt Current System (NHCS) off Peru <sup>21,22</sup> represents a unique  
97 ecosystem to explore the influence of ocean warming on marine biogeochemistry and ecology  
98 in the context of the climate forcing induced by El Niño Southern Oscillations (ENSO) <sup>22</sup>. The  
99 NHCS is one of the most productive regions of the global ocean <sup>23</sup>, exhibiting the most  
100 extensive and shallow OMZ <sup>22,24</sup> on earth, and accounting for >10% of global fisheries, and  
101 particularly anchovy (*Engraulis ringens*) <sup>23</sup>. The shallow oxycline (~20–100 m) acts as a  
102 physical barrier for fish biomass, which is mostly concentrated at the surface. The oxycline is  
103 also the relevant interface for the formation of MeHg. A high proportion of dissolved MeHg  
104 (relative to total Hg) has been documented in this region in surface waters compared to other  
105 parts of the Pacific Ocean <sup>25,26</sup>. Every 2–7 years, ENSO events strongly affect marine primary  
106 productivity and food web dynamics. During extreme Eastern Pacific (EP) El Niño events, the  
107 reduced wind speed along the Peruvian coast leads to a decreased upwelling circulation that  
108 brings normally deep cold nutrient rich waters to the surface sustaining the high productivity of  
109 this region <sup>21</sup>. Under El Niño conditions, the thermocline, nitracline and oxycline deepen  
110 significantly and the water column becomes more oxygenated at the surface, leading to warmer  
111 surface temperature anomalies <sup>24</sup>. Under these circumstances, the food web is particularly

112 affected since the phytoplankton growth is strongly reduced. This impacts the whole ecosystem  
113 leading to a reduced fish biomass potentially influencing the food web structure, causing a high  
114 mortality of marine top predators<sup>27</sup>, but also impacting fishery catch<sup>28,29</sup>.

115 In this work, we investigated how climate forcing induced by ENSO in the NHCS,  
116 influences MeHg biogeochemistry and concentrations at the top of the marine food web. We  
117 hypothesized that the warming conditions and the deepening of the oxycline during El Niño  
118 events would change the depth at which MeHg is produced, likely decreasing its  
119 photodegradation, possibly favouring its production, bioavailability and concentration further  
120 in the food chain. We also explored and discussed how complementary and compensating  
121 processes could mitigate the production of MeHg and its concentration in the food chain during  
122 these events due to the reduced vertical export of organic matter toward the oxycline. Our  
123 strategy consisted of documenting and discussing the role of ENSO through the change of the  
124 environmental, physical and oceanic biogeochemical variables on Hg concentrations and Hg  
125 stable isotopic composition in a 8 year time series of blood samples from two key sentinel avian  
126 top predators: the Peruvian booby *Sula variegata* and the Guanay cormorant *Phalacrocorax*  
127 *bougainvillii*, that are known to feed almost exclusively (90% on average) on anchovy<sup>30,31</sup>.  
128 Mercury concentration in seabird blood has been documented to be a very sensitive proxy of  
129 MeHg levels and bioavailability in the local and regional marine ecosystem<sup>32,33</sup>. Blood Hg  
130 isotopic composition of seabirds efficiently reflects recent Hg exposure<sup>34</sup> (i.e. 2-5 weeks  
131 preceding sampling<sup>35</sup>), and can provide major clues to elucidate the marine Hg cycle<sup>36,37</sup>.  
132 Mercury stable isotopes has greatly improved knowledge on the sources of exposure, transfer  
133 pathways, and metabolism of Hg in marine consumers<sup>36,38,39</sup>. Many abiotic (e.g.  
134 photoreduction, volatilization)<sup>40,41</sup> and biotic processes (e.g. methylation, demethylation)<sup>42-44</sup>  
135 result in mass-dependent isotope fractionation (MDF, reported as  $\delta^{202}\text{Hg}$ ). By contrast, mass-  
136 independent fractionation of odd-mass number isotopes (odd-MIF, reported as  $\Delta^{199}\text{Hg}$  or

137  $\Delta^{201}\text{Hg}$ ) has been primarily observed during aquatic photochemical reactions <sup>40</sup>, and is  
138 preserved during biological or trophic processes <sup>45</sup>. The systematic decline in  $\Delta^{199}\text{Hg}$  observed  
139 in marine organisms with the depth at which they feed has been attributed to the decrease of  
140 MeHg photodegradation in the water column, allowing to demonstrate that MeHg is mainly  
141 produced in the OMZ <sup>38</sup>. This proxy is thus particularly relevant in the context of the present  
142 study. Carbon ( $\delta^{13}\text{C}$ ) and nitrogen ( $\delta^{15}\text{N}$ ) stable isotopes were also determined to provide  
143 insights about the foraging ecology of the seabird species, and to detail the influence of isotopic  
144 baseline variations during contrasted upwelling regimes <sup>46-49</sup> on Hg concentrations and stable  
145 isotopes.

146

## 147 **2 Materials and methods**

### 148 2.1 Sample collection

149 Sampling was conducted from 2009 to 2016 (except 2014) during the months of October-  
150 November at Pescadores Island, Peru ( $11^{\circ}46'\text{S}$ ,  $77^{\circ}15'\text{W}$ ) which correspond to the breeding  
151 period. During that time, seabirds are restricted to their nesting area making Hg concentrations  
152 and stable isotope data only representative of their breeding grounds in the NHCS. Individuals  
153 of Guanay cormorants and Peruvian boobies were randomly chosen during each sampling  
154 campaign. Each bird was measured, weighed and sexed as detailed in a previous work <sup>31</sup>. Birds  
155 were breeders (breeding 1-4 weeks old chicks at the time of sampling) or juveniles. Some  
156 individuals of boobies and cormorants were equipped with GPS recorders for spatial tracking  
157 of their foraging trips and time-depth recorders to track their diving behaviour <sup>31</sup>. The two  
158 seabird species slightly differ on their foraging strategies in terms of diving depths, with  
159 cormorants presenting better diving capacities than boobies <sup>31</sup>. No sex-related differences in  
160 foraging habits have been observed between males and females of the two species <sup>31</sup>. Blood

161 samples were collected from a wing or tarsal vein and preserved in 70% ethanol <sup>49</sup>. Samples of  
162 ingested anchovies (standard length of 12-13 cm) were also collected and preserved similarly  
163 in 70% ethanol when the birds regurgitated spontaneously. No other prey was observed. Prior  
164 analysis, blood and prey samples were dried, lyophilized and grounded. The number of seabird  
165 individuals and prey analysed for Hg concentrations, C, N isotope analysis ranged from 5 to 41  
166 individuals per species depending on the year, while Hg isotope analysis was performed in 4 to  
167 10 chosen individuals, per species per year, based on the sample mass available.

168

## 169 2.2 Analytical methods

### 170 **Total Hg concentrations**

171 Total Hg concentrations, hereafter expressed in  $\mu\text{g g}^{-1}$  of dry weight (dw), were quantified by  
172 using a DMA80 analyzer (Milestone, USA). The detection limit was  $0.005 \mu\text{g}\cdot\text{g}^{-1}$  dw. Three  
173 certified reference materials were analysed for evaluation of accuracy and reproducibility of  
174 our methods: tuna fish muscle (ERM-CE-464 and IAEA-436) and lobster hepatopancreas  
175 material (TORT-3); providing a respective accuracy of  $96\pm 12\%$  (n=15),  $96\pm 9\%$  (n=6), and  
176  $100\pm 9\%$  (n=6) relative to recommended reference values. Internal homemade blood reference  
177 material (red blood cells, RBC-KP) was also used for validation of seabird blood analyses and  
178 provided an accuracy of  $96\pm 6\%$  (n=3) relative to previously published values, as detailed  
179 elsewhere <sup>34</sup>.

### 180 **Total Hg isotopic analyses**

181 Blood samples (0.05–0.10 g) were soaked in 3 or 5 mL of concentrated bi-distilled  $\text{HNO}_3$   
182 ( $\sim 11\text{N}$ ) overnight at room temperature then heated on a hotplate at  $80^\circ\text{C}$  during 6 h (4 h in  
183  $\text{HNO}_3$  and 2 h more after addition of 1/3 of the total volume of  $\text{H}_2\text{O}_2$  30%, ULTREX quality).  
184 We added 100  $\mu\text{L}$  of  $\text{BrCl}$  ( $0.2 \text{ mol L}^{-1}$ ) to convert all MeHg to inorganic Hg. The digest



185 mixtures were finally diluted in inverse aqua regia (3 HNO<sub>3</sub>: 1 HCl). Final Hg concentrations  
186 ranged from 0.5 to 1 ng·g<sup>-1</sup>.

187 Mercury isotopic composition was measured using a multicollector inductively coupled  
188 to plasma mass spectrometry (MC-ICP-MS, Thermo Finnigan Neptune Plus) with continuous-  
189 flow cold vapor (CV) generation using Sn (II) reduction (CETAC HGX-200). Mercury isotopic  
190 values were reported as delta notation, calculated relative to the bracketing standard NIST  
191 SRM-3133 reference material to allow interlaboratory comparisons, as described in the SI.  
192 Secondary standard NIST RM-8160 (previously UM-Almadén standard) was used for  
193 validation of the analytical session (Table S1). Recoveries of extraction (102±17%, mean±SD)  
194 were calculated for all samples (n=87) by checking the signal intensity obtained on the MC-  
195 ICPMS for diluted extracts relative to NIST 3133 standard (with an approximate uncertainty of  
196 ±15%). Certified reference materials (ERM-CE-464 and IAEA-436) and the internal blood  
197 reference material (RBC-KP) were also measured (Table S1). Uncertainty for delta values was  
198 based on 2SD errors for each certified reference material (Table S1).

### 199 **Carbon and nitrogen stable isotopic analyses**

200 Blood samples were freeze-dried and powdered, and subsamples were weighed with a  
201 microbalance and packed in tin containers. Carbon and nitrogen stable isotope ratios were  
202 determined in total seabird blood and anchovies with a continuous flow mass spectrometer  
203 (Delta V Advantage with a ConFlo IV interface, Thermo Scientific, Bremen, Germany) coupled  
204 to an elemental analyser (Flash EA1112, Thermo Scientific, Milan, Italy). Results are in delta  
205 notation relative to Vienna PeeDee Belemnite and atmospheric N<sub>2</sub> for δ<sup>13</sup>C and δ<sup>15</sup>N,  
206 respectively. Replicate measurements of internal laboratory standards (acetanilide) indicated  
207 measurement errors <0.15‰ for both δ<sup>13</sup>C and δ<sup>15</sup>N values.

### 208 2.3 Environmental parameters

209 The spatio-temporal variability of the main marine physical and biogeochemical parameters of  
210 seabird foraging areas was derived from satellite and acoustic observations. Satellite datasets  
211 of sea-surface temperature (SST), net primary productivity (NPP), wind speed, diffuse  
212 attenuation coefficient  $K_d490$ , photosynthetically available radiation (PAR), total kinetic  
213 energy (TKE) and upwelling index (Ekman transport), were integrated at three different spatial  
214 scales, respectively from the coast to 80, 100 and 150 km offshore: small-scale A1 (lat: 12.5-  
215 11.0°S); medium-scale A2 (lat: 13.5-10.5°S) and large-scale A3 (lat: 14.0-9.5°S). The small-  
216 scale spatial integration (A1) is based on the tracking data of the main seabird trajectories <sup>31</sup>  
217 and reflects their effective foraging zone (Figure 1). We know that seabirds are restricted to  
218 foraging areas near their colonies during their breeding period due to the need to frequently  
219 feed their chicks. However, since MeHg accumulated in seabirds is mainly transferred from  
220 anchovies that integrate larger areas <sup>50,51</sup>, we also treated the environmental data at large scale  
221 area (A3) based on anchovy biomass distribution <sup>50,52</sup> for the considered period. Medium-scale  
222 area A2 was also considered as an intermediate area between A1 and A3 (Figure S1).

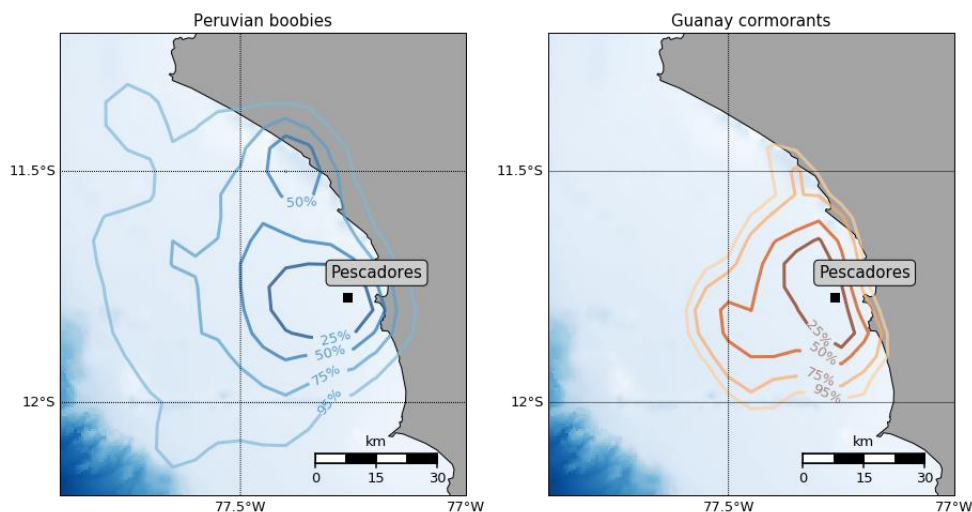
223 Seabird blood represents exposure over the last 2 to 5 weeks preceding sampling <sup>34</sup>, i.e.  
224 October-November. We therefore calculated mean values (and standard error, SE) of each  
225 environmental parameter for the period from the 1<sup>st</sup> October to 30<sup>th</sup> November. All  
226 environmental satellite variables were averaged at monthly resolution. Anomalies of the  
227 environmental variables were calculated relative to mean seasonal values for the 2009-2016  
228 period.

229 Oxycline depth variations were recorded by acoustic measurements based on the depth  
230 of the vertical extension of the epipelagic community as explained in previous work and specific  
231 for this area <sup>53</sup>. Acoustic oxycline data were previously compared and validated with *in situ*  
232 dissolved oxygen concentration analyses from the period October-December in Callao station

233 (estimation of oxycline at  $DO=22 \mu\text{mol Kg}^{-1}$ , see <sup>22,54</sup> for more details). Acoustic data used in  
234 this work were processed at the three integrated areas A1, A2 and A3 with respective spatial  
235 resolutions (0.5, 1 and 2 degrees and 50 meters of acoustic data resolution) and integrated  
236 during the period of October to November. Acoustic data of 2013 were only available for the  
237 period February-April, so we estimated the oxycline depth values for October-November 2013  
238 by extrapolation validated with the correlation between oxycline depth and SST anomalies for  
239 the three spatial areas.

240 Anchovy total biomass (mean  $\pm$  SE) was determined by acoustic observations and  
241 integrated for a large spatial coastal area (8 to 16°S) corresponding to the spring survey  
242 (October-November) using the methodology developed by Simmonds and co-workers <sup>55</sup>. Data  
243 of anchovy fish captures were provided by the FAO (Food and Agriculture Organization of the  
244 United Nations <sup>56</sup>) for the Major Fishing Area in the southeast Pacific Ocean and by the Ministry  
245 of Production of Peru <sup>57</sup>. The variability of ENSO was determined by the ICEN (Coastal El  
246 Niño Index), which is a regional (Eastern Pacific) index of ENSO activity in the region of Peru  
247 provided by the Technical Committee of the National Study of the El Niño Phenomenon  
248 (ENFEN) <sup>58</sup>

249



250

251 **Figure 1. Seabird foraging area over the 2009-2015 period: kernel of dive density estimations for boobies**  
252 **(left panel) and cormorants (right panel).**

253

#### 254 2.4 Statistical tests

255 Statistical analyses were performed using the software R 3.3.2<sup>59</sup>. Data were first checked for  
256 normality of distribution and homogeneity of variances using Shapiro–Wilk and Breusch-Pagan  
257 tests, respectively. Statistical significance of the temporal variations of Hg concentrations, C,  
258 N and Hg isotopic composition were examined using a linear regression fitted along years.  
259 Statistical differences between years were investigated by non-parametrical tests (Kruskal–  
260 Wallis with Conover-Iman post-hoc test) since data did not meet specificities of normality and  
261 homoscedasticity. Interspecies differences were also tested statistically by Wilcoxon tests.  
262 Statistical significance was set at  $p < 0.05$ .

263 We used generalized additive models (GAM)<sup>60</sup> to assess the influence of environmental  
264 parameters in explaining the interannual variations of seabird Hg concentrations and isotopic  
265 signatures of the NHCS. GAM tests were fitted in R using the mgcv package<sup>61</sup>. Response  
266 variables (blood Hg concentrations converted into  $\log(\text{Hg})$ ,  $\delta^{202}\text{Hg}$  and  $\Delta^{199}\text{Hg}$  values were  
267 assumed to follow a Gaussian distribution. Explanatory variables tested included ecological  
268 factors ( $\delta^{15}\text{N}$  and  $\delta^{13}\text{C}$  values) and oceanographic parameters (oxycline depth, SST, ICEN  
269 index, chlorophyll-a concentration, NPP, wind speed, diffuse attenuation coefficient  $K_d490$ ,  
270 PAR, coastal upwelling index, TKE and anchovy biomass). Multi-collinearity was checked by  
271 calculation of the variance inflation factor (VIF)<sup>62</sup>. Only the parameters whose  $\text{VIF} < 2$  were  
272 considered in the GAM models. ICEN index was found to be collinear to other variables and  
273 was removed from the explanatory variables. Chlorophyll-a concentrations, PAR and NPP were  
274 highly correlated, so we only tested these variables separately in the GAM models. All the  
275 explanatory variables were fitted in the GAM with a low spline complexity ( $k = 3$ ) to reduce

276 over-fitting. The best-fit GAM models were selected by using the Akaike's Information  
277 Criterion (AICc) corrected for small samples sizes <sup>60</sup>. Additionally, we examined the fitted  
278 GAM models with diagnostic plots of residuals. To determine the amount of variation explained  
279 by each explanatory variable, we fitted a separate model for individual variable. The deviance  
280 explained (% DE) for each model was compared to assess the capacity of prediction of each  
281 model. Results of GAM tests are included in the SI ([Table S2](#)).

## 282 **3 Results & discussion**

### 283 3.1 Humboldt ENSO events: physical and biogeochemical dynamics

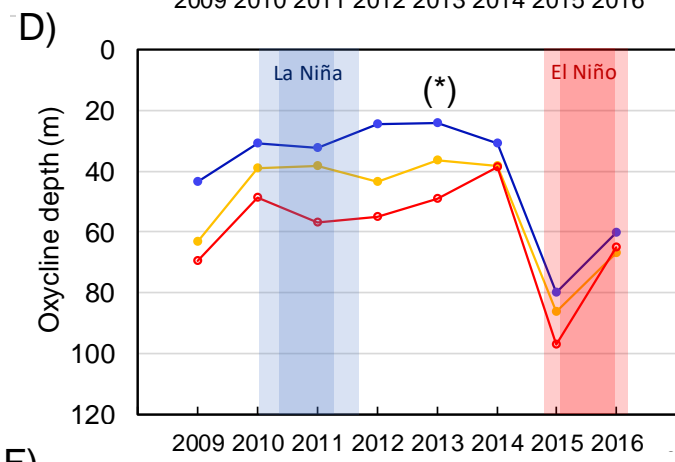
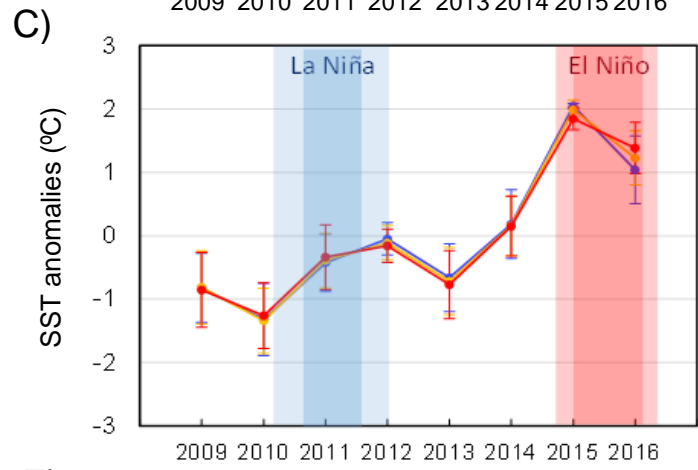
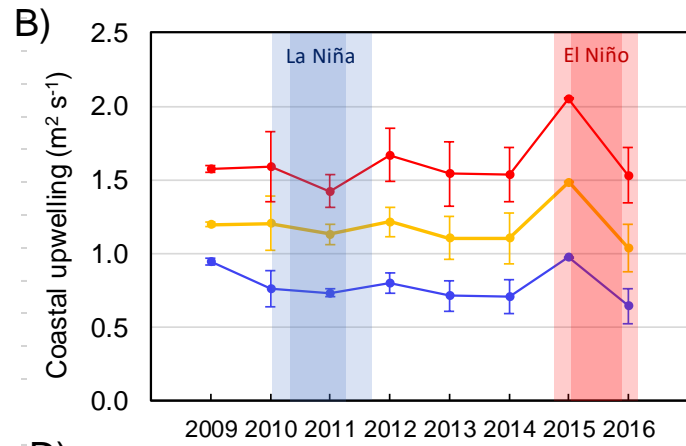
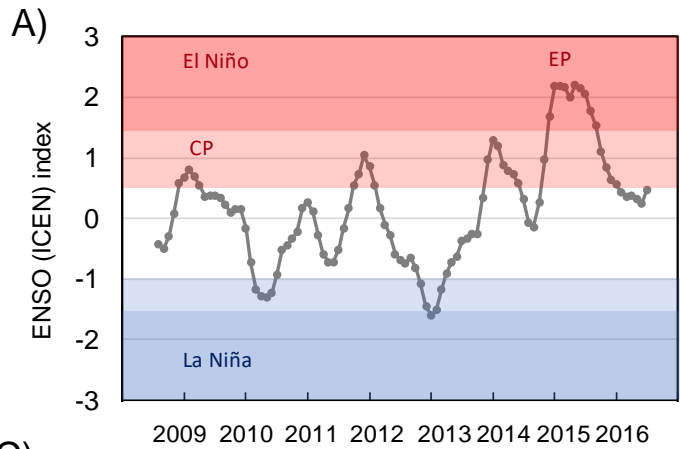
284 Monthly-averaged ICEN index shows the ENSO variability for the period 2009-2016 ([Figure](#)  
285 [2A](#)). The intensity of the events (weak, moderate, strong) was also based on the ICEN index  
286 diagnostic of the ENFEN <sup>58,63</sup>. The impact of a given ENSO event on the Peruvian upwelling  
287 system depends on its magnitude and the spatial structure. El Niño events that develop in the  
288 Central-Pacific (called CP El Niño or Modoki) do not induce significant warming of the surface  
289 waters off the shelf of Peru, contrary to extreme and Eastern Pacific El Niño events (EP El  
290 Niño) <sup>64,65</sup>. The definition used for the ENFEN to classify extreme ENSO events requires the  
291 registration during more than three consecutive months of an ICEN index  $> 1$  °C for El Niño  
292 and  $< -1.2$  °C for La Niña events <sup>58,63</sup>. The period of 2009-2010 was classified as a weak CP El  
293 Niño (ICEN index of 0.7 °C) exhibiting a very limited influence on the Peruvian coast <sup>29</sup>, so  
294 was not considered in this study. However, an extreme EP El Niño occurred during the 2015-  
295 2016 period (ICEN index of 2.2 °C) affecting the NHCS. The period from mid-2010 to early  
296 2011 was classified as a moderate La Niña event (ICEN index of  $-1.3$  °C).

297 Despite a medium but sustained yearly upwelling intensity during the study period, a  
298 relatively high persistent upwelling index was observed in late 2015 ([Figure 2B](#)). Positive SST  
299 anomalies ( $\approx +2^\circ\text{C}$ ) were observed both in 2015 and 2016, which corresponds to the signature

300 of extreme EP El Niño conditions (Figure 2C). The warming of surface waters during El Niño  
301 is caused by downwelling equatorial Kelvin waves generated by wind anomalies in the western  
302 equatorial Pacific<sup>66</sup>. During El Niño events, the relatively warmer and deeper mixed layer  
303 decreases water ventilation and upwelling of deep cold-water masses is reduced which  
304 translates into a significant deepening of the oxycline in our study area (from 40 to ~90 m depth)  
305 in 2015 (Figure 2D), whereas in normal conditions the oxycline depth (OMZ=22  $\mu\text{mol Kg}^{-1}$ )  
306 oscillates between 15 to 25 m depth<sup>24</sup>. This strong vertical deepening of the oxycline is in  
307 agreement with previous observations<sup>54,67</sup> and consistent with El Niño peak phase (November-  
308 December 2015).

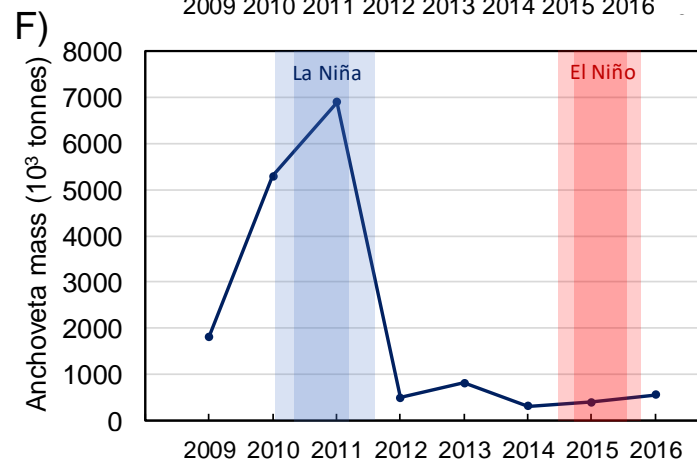
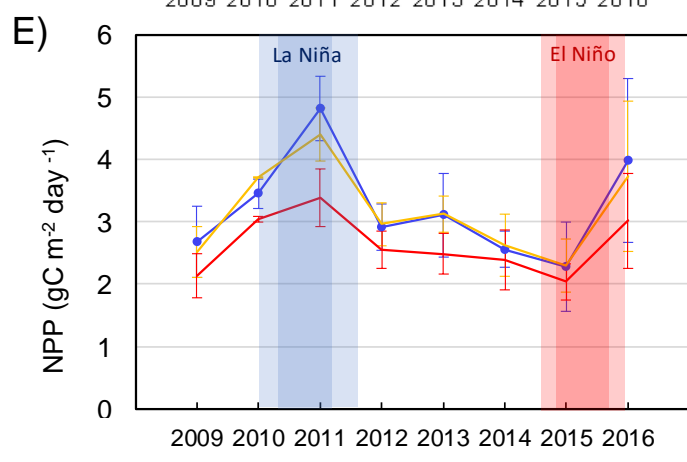
309         The NPP off the Peruvian upwelling system was relatively stable during the period  
310 2009-2016 and varied within the typically observed ranges for this ecosystem (1.8 to 5.2 g C  
311  $\text{m}^{-2} \text{day}^{-1}$ ,<sup>68</sup>) (Figure 2E). El Niño 2015-2016 did not strongly impact primary production in  
312 the eastern Pacific, compared to past extreme EP El Niño events<sup>69</sup>. During La Niña 2010-2011,  
313 the average NPP during the spring period exhibited a maximum, particularly in the spatial area  
314 near the coast A1 (4.8 gC  $\text{m}^{-2} \text{day}^{-1}$ ). This year also accounted for an exceptionally large  
315 anchovy biomass (~7 million tonnes). On average, enhanced global biomass of approximately  
316 +1.1 million tonnes are observed during strong La Niña years<sup>29</sup>. In contrast, EP and extreme  
317 El Niño events commonly result in reduced global landings, with anomalies of -0.7 to -3.2  
318 million tonnes depending on the intensity of the event (Figure 2F)<sup>29</sup>. Therefore, strong El Niño  
319 conditions in 2015-2016 and La Niña event occurring in 2010-2011 resulted in strong  
320 variability of climatic conditions of the Peruvian ecosystem, with SST anomalies of  $\pm 3^\circ\text{C}$ ,  
321 oxycline variability from 20 to 100 m depth and large range of NPP and biomass gradients.

322



Integration areas

- A1
- A2
- A3



324 **Figure 2. Interannual variations of 2-month means (1<sup>st</sup> October to 30<sup>th</sup> November) of physical and**  
325 **biogeochemical/biological parameters measured in the Humboldt upwelling region. A) ENSO index (as**  
326 **regional Coastal El Niño index, ICEN): El Niño event in red (CP and EP refer respectively to Central Pacific**  
327 **and Eastern Pacific El Niño events) and La Niña event in blue, B) Coastal upwelling index ( $\text{m}^2 \text{s}^{-1}$ , Ekman**  
328 **transport), C) Sea surface temperature anomalies ( $^{\circ}\text{C}$ ), D) Oxycline depth (m), E) Net primary production**  
329 **( $\text{mg C}\cdot\text{m}^{-2}\cdot\text{day}^{-1}$ ), F) Anchoveta total biomass (in  $10^3$  tons). Values are means  $\pm$  standard error for the total**  
330 **number of observations over the 2-month period. (\*) Values of oxycline depth for 2013 for the period**  
331 **October-November are estimated by extrapolation from the correlation of recorded SST anomalies and**  
332 **oxycline depth data available for the period February-April 2013.**

333

### 334 3.2 Relation of seabird isotopes to their specific foraging habits.

335 Similar to previous works, we assumed here that total Hg concentration and Hg isotopic  
336 composition in seabird blood represent the dominant (>90%) MeHg fraction<sup>36,37</sup>. Overall blood  
337 Hg concentrations (mean  $\pm$  SD; min-max) were consistently higher in Guanay cormorants ( $0.86$   
338  $\pm 0.34$ ;  $0.23$ - $1.81 \mu\text{g} \cdot \text{g}^{-1}$ ,  $n=118$ ) than in Peruvian boobies ( $0.57 \pm 0.21$ ;  $0.13$ - $1.29 \mu\text{g} \cdot \text{g}^{-1}$ ,  
339  $n=110$ ) for the period considered (Wilcoxon test,  $p<0.001$ ). Fieldwork revealed almost no other  
340 preys than anchovy in seabird regurgitate, confirming that both Guanay cormorants and  
341 Peruvian boobies mainly prey upon anchovies with a similar relative importance of 81–96%  
342 and 80–93% of their diets, respectively<sup>30,70</sup>. The offset of blood Hg levels between the two  
343 species may be due to slight differences in their foraging habits and/or or species-specific  
344 metabolic response to Hg<sup>36,71</sup>.

345 A decreasing trend of  $\delta^{13}\text{C}$  values from coastal to oceanic zones is commonly observed  
346 in many marine ecosystems, including the Peruvian upwelling system<sup>46</sup>, because  $\delta^{13}\text{C}$  values  
347 of particulate organic matter decrease from inshore to offshore waters due to the reduction of  
348 productivity<sup>68,72</sup>. Consistently lower  $\delta^{13}\text{C}$  values of Guanay cormorants relative to Peruvian  
349 boobies ( $p<0.001$ ) over the studied period (Figure S4) are therefore consistent with cormorants  
350 using more inshore foraging habitats, as shown in Figure 1. Guanay cormorants are known to  
351 have excellent diving capacities up to 32 m depth<sup>31</sup>, then covering potentially the deep vertical  
352 range of the anchovy aggregations, while Peruvian boobies target the extended horizontal range



353 of anchovy schools<sup>31,73</sup>. Similarly,  $\delta^{13}\text{C}$  values of particulate organic matter are related to water  
354 depth<sup>74</sup> so the vertical foraging habitats of seabirds could also influence their C isotopic values,  
355 in line with the distribution of anchovy schools distributed above the oxycline<sup>75</sup>.

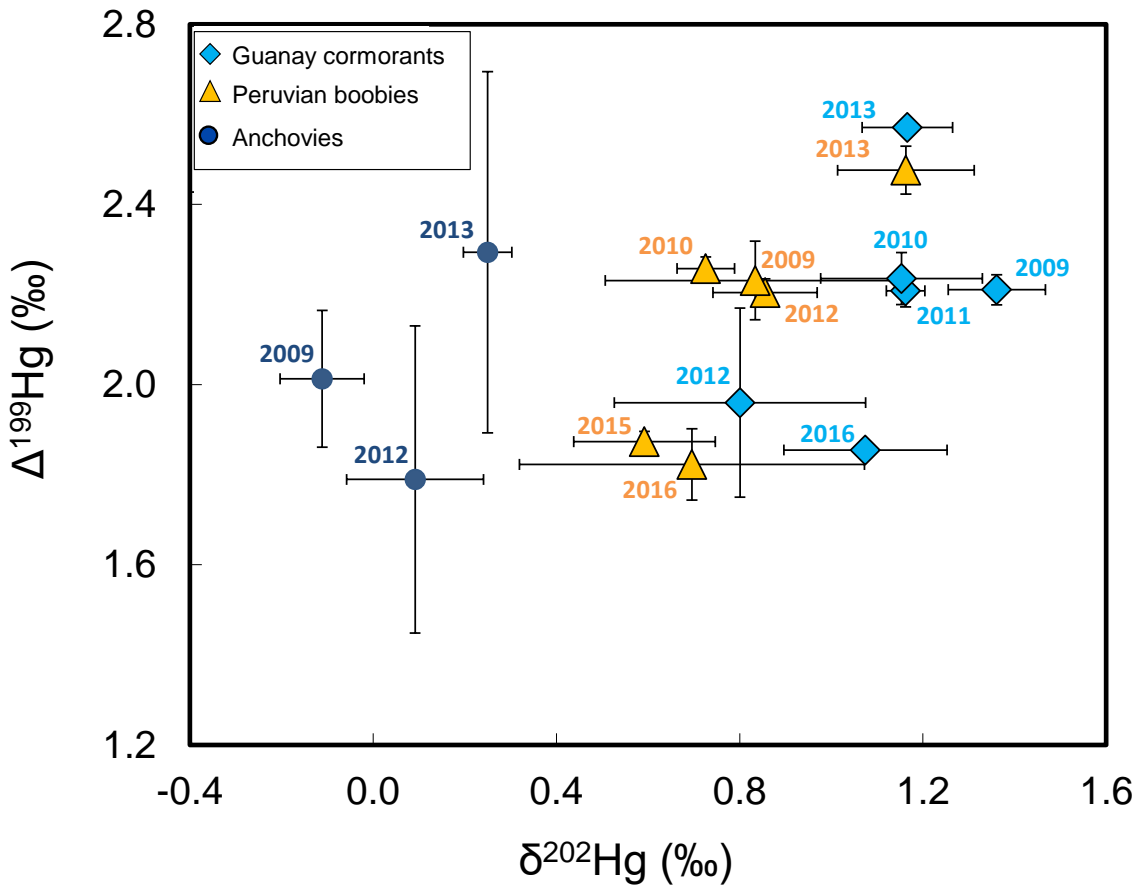
356 Guanay cormorants presented only slightly higher  $\delta^{15}\text{N}$  values (0.2 to 0.5‰ of mean  
357 difference) than Peruvian boobies (Wilcoxon test,  $p < 0.001$ ), except in 2016. This suggests that  
358 the two seabird species forage at a near similar trophic level and on very close prey items. The  
359 limited but significant differences in both  $\delta^{13}\text{C}$  and  $\delta^{15}\text{N}$  among the two-seabird species could  
360 reflect slight variations of their foraging habits and specialisation in line with the variability of  
361 the aggregation and distribution of anchovy schools between the surface and the oxycline.  
362 Differences in seabird metabolism could also explain the slight differences observed, as for Hg.  
363 However, these results confirm that both seabird species forage essentially on anchovy schools  
364 (Figure S4) confirming the field work observations by our team<sup>30,70</sup>. As detailed in section 3.4,  
365 we found that during el Niño events, a reduced denitrification associated with a deeper oxycline  
366<sup>76</sup> is mostly responsible for the interannual differences in  $\delta^{15}\text{N}$  in seabirds, and for the rest of  
367 the food web<sup>48</sup>.

368 Individual bird blood  $\delta^{202}\text{Hg}$  (MDF) showed moderate variability both for Guanay  
369 cormorants (0.41-1.49‰) and Peruvian boobies (0.28-1.37‰). Overall, the two species  
370 presented statistically different  $\delta^{202}\text{Hg}$  values (Kruskal Wallis,  $H=8.144$ ,  $p=0.004$ ), especially  
371 during 2009 and 2010 in which cormorants displayed 0.5‰ higher mean values than boobies  
372 (Figure 3). Significant correlation between Hg concentration and  $\delta^{202}\text{Hg}$  values was observed  
373 in seabirds ( $R^2=0.51$ ,  $p < 0.0001$ ,  $n=72$ , Figure S7) although it was not significant for anchovies  
374 ( $p=0.06$ ,  $n=14$ ). Mass dependent fractionation of Hg isotopes occurs during many physical,  
375 chemical or biological processes<sup>41,77-79</sup>. The influence of biological and ecological factors on  
376  $\delta^{202}\text{Hg}$  values shows the limitation of this type of signature to trace which Hg transformations  
377 occur during ENSO-related variations. The interpretation of seabird  $\delta^{202}\text{Hg}$  values as a proxy

378 of changing environmental conditions requires a complete knowledge of all the processes and  
379 factors driving Hg MDF, especially when using biological models such as seabirds (i.e., trophic  
380 ecology and intrinsic metabolic/physiological processes). For instance, seabird  $\delta^{202}\text{Hg}$  values  
381 are known to be sensitive to their specific foraging habitats <sup>36</sup>. Higher Hg concentrations and  
382  $\delta^{202}\text{Hg}$  values of Guanay cormorants support that this species targets larger size and deeper  
383 anchovy aggregations than Peruvian boobies. Both seabird species exhibited significantly  
384 higher  $\delta^{202}\text{Hg}$  values than anchovy (mean difference of 0.9‰). This is in good agreement with  
385 the Hg MDF commonly observed in predator-prey and is thought to reflect the partial metabolic  
386 breakdown of MeHg, which leads to bioaccumulation of isotopically heavier MeHg in birds,  
387 sharks and mammals <sup>42,80,81</sup>. The lower blood Hg levels in Peruvian boobies are accompanied  
388 by lower  $\delta^{202}\text{Hg}$  (i.e. less demethylated MeHg), suggesting that species-specific metabolic  
389 MeHg breakdown is not a major control factor on blood Hg.

390 We observed similar variability of  $\Delta^{199}\text{Hg}$  (Hg odd-MIF) between Guanay cormorants  
391 (1.63-2.60‰) and Peruvian boobies (1.70-2.57‰) (Kruskal Wallis,  $H=2.117$ ,  $p=0.146$ ).  
392 Positive  $\Delta^{199}\text{Hg}$  in aquatic food webs are mainly due to the photochemical processes prior to  
393 MeHg incorporation into food webs, then preserving the  $\Delta^{199}\text{Hg}$  baseline signature <sup>40</sup>. This is  
394 confirmed by the  $\Delta^{199}\text{Hg}/\Delta^{201}\text{Hg}$  of  $1.15\pm 0.09$  (SE) of anchovy and  $1.02\pm 0.05$  (SE) of seabirds  
395 (Figure S5). Overall  $\Delta^{199}\text{Hg}$  values of anchovies ( $2.04\pm 0.37\%$ ,  $n=14$ ) were similar to  $\Delta^{199}\text{Hg}$   
396 values of seabirds ( $2.08\pm 0.24\%$ ,  $n=72$ ) ( $H=4.89$ ,  $p=0.09$ ), which is coherent with the absence  
397 of Hg odd-MIF during trophic transfer <sup>45</sup>, and confirms that the seabirds feed predominantly on  
398 anchovy. A consistent decrease of fish  $\Delta^{199}\text{Hg}$  with the foraging depth has been observed in the  
399 open Pacific ocean due to the dilution of surface photodegraded MeHg by in situ methylated  
400 Hg at depth <sup>38</sup>. Although the two seabird species slightly differ in their foraging depth <sup>31</sup>, their  
401 similar  $\Delta^{199}\text{Hg}$  values suggest that both accumulate MeHg that has undergone similar degrees

402 of photodemethylation in the water column confirming that both species rely on similar  
 403 anchovy aggregations.



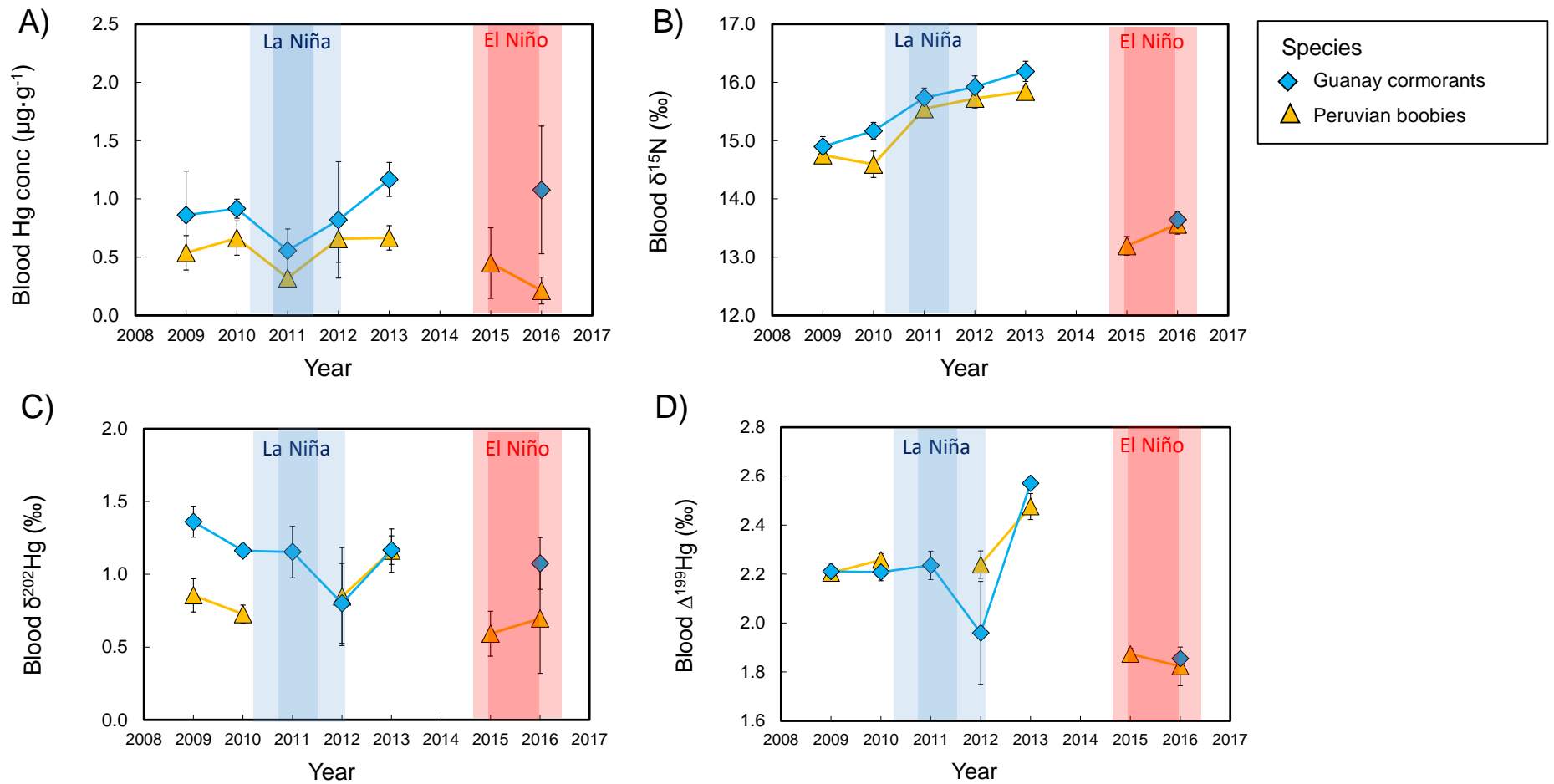
404  
 405 **Figure 3. Annually averaged values of Hg odd-MIF versus Hg MDF values ( $\Delta^{199}\text{Hg}$  versus  $\delta^{202}\text{Hg}$ ) of seabirds**  
 406 **(2009-2016) and anchovies (2009, 2012, 2013). Values are means $\pm$ SD. Number of individuals: n=4-10 per**  
 407 **species per year).**

408  
 409 **3.3 Limited influence of ENSO forcing on seabird blood Hg concentrations.**

410 Significant interannual blood Hg variability was observed for both Guanay cormorants and  
 411 Peruvian boobies (Kruskal-Wallis, H=48.3 and 55.4, respectively, both  $p < 0.0001$ ). In 2013,  
 412 cormorants exhibited significantly higher mean Hg concentrations ( $1.17 \pm 0.15 \mu\text{g} \cdot \text{g}^{-1}$ ) than the  
 413 rest of the years. Guanay cormorants and Peruvian boobies showed statistically lower  
 414 concentrations in 2011 ( $0.56 \pm 0.19$  and  $0.32 \pm 0.05 \mu\text{g} \cdot \text{g}^{-1}$ , respectively), and during 2016,

415 Peruvian boobies exhibited their lowest concentration of  $0.21 \pm 0.12 \mu\text{g} \cdot \text{g}^{-1}$ . Mercury  
416 concentrations of anchovies (muscle) were highly variable during the period 2009-2013 ( $0.08$   
417  $\pm 0.05$ ,  $0.01$ - $0.23 \mu\text{g} \cdot \text{g}^{-1}$ ,  $n=66$ ) but did not show significantly different Hg concentration  
418 among years (Kruskal-Wallis,  $H=22.65$ ,  $p=0.001$ ) (Figure S6). When applying GAMs, the  
419 optimal model to explain the variability of Hg concentration, expressed as  $\log(\text{Hg})$ , was the  
420 model including anchovy biomass, blood  $\delta^{15}\text{N}$  and upwelling index together as explanatory  
421 variables (Table S2). However, this model only explained for 27 to 30% of the interannual Hg  
422 concentration trends, depending on the spatial area considered. This suggests a weak impact of  
423 the changing biogeochemical parameters on the MeHg levels at the top of food web during  
424 contrasted climatic conditions occurring on the period 2009-2016.

425 A recent study in the Galapagos archipelago also reported low interannual variations of  
426 feather Hg concentrations in several species of booby *Sula spp.* during the period 2011-2017  
427 <sup>82</sup>. This strengthens our finding, at a much larger regional scale, showing the absence of a  
428 significant change in MeHg concentrations of third-level consumers of the marine food web  
429 under strong climate forcing conditions. The relatively stable MeHg concentrations observed  
430 in seabirds during ENSO events of high amplitude contrast with tentative modelling and  
431 experimental studies which suggested higher MeHg bioaccumulation rates in fish with  
432 increasing water temperatures <sup>9,19,20</sup>. Schartup et al. <sup>9</sup> predicted that a  $1^\circ\text{C}$  increase of seawater  
433 temperature would lead to a 32 and 70% increase of MeHg concentrations in Atlantic cod and  
434 spiny dogfish, respectively. The same authors also suggested that dietary changes in pelagic  
435 fish in response to overfishing could lead to changes in MeHg bioaccumulation rates <sup>9</sup>.  
436 Contrarily, our results show that an increase of seawater temperature of  $2^\circ\text{C}$  during El Niño  
437 2015-2016 (which can reach  $+3^\circ\text{C}$  range in extreme El Niño cases <sup>83</sup>) did not translate into a  
438 significant impact on MeHg concentrations in top predators of the Peruvian food web,  
439 represented here by seabirds.



440

441 **Figure 4. Interannual variations of seabird blood A) Hg concentrations ( $\mu\text{g} \cdot \text{g}^{-1}$ , dw); B) N isotopes ( $\delta^{15}\text{N}$ , ‰); C) Hg MDF ( $\delta^{202}\text{Hg}$ , ‰); D) Hg odd-MIF ( $\Delta^{199}\text{Hg}$ , ‰).**  
 442 **Values are Means  $\pm$  SD. Number of individuals analysed: blood Hg concentration and  $\delta^{15}\text{N}$  values (5-41 individuals per species per year), Hg isotope analysis (4-10**  
 443 **individuals, per species per year).**

#### 444 3.4 ENSO driven variability of nitrogen isotopes

445 **Figure 4B** shows the progressive increase of seabird  $\delta^{15}\text{N}$  values from 2010 to 2013, which  
446 reached the highest mean values in 2013, both for Guanay cormorants and Peruvian boobies  
447 ( $16.19 \pm 0.17$  and  $15.84 \pm 0.09\text{‰}$ , respectively). In contrast,  $\delta^{15}\text{N}$  values of seabirds decreased  
448 sharply in 2015 (boobies:  $13.19 \pm 0.16\text{‰}$ ) and 2016 (cormorants:  $13.64 \pm 0.14\text{‰}$  and boobies:  
449  $13.56 \pm 0.17\text{‰}$ ) during the El Niño event. We observed significant interannual variations of  
450 blood  $\delta^{15}\text{N}$  values of cormorants and boobies (Kruskal Wallis,  $H=91.3$  and  $97.8$  respectively,  
451 both  $p<0.0001$ ). Interestingly, the observation of a limited interspecies difference in  $\delta^{15}\text{N}$  (0.2  
452 to 0.5‰) among all years, in the context of following similar and parallel interannual trends  
453 capturing the exact same  $\delta^{15}\text{N}$  drop of  $\sim 2.5\text{‰}$  in 2015-2016 (which corresponds in theory to a  
454 change close of one trophic level) is inconsistent with the idea that it might be caused by a  
455 change in diet for the two seabird species. The vertical movements of anchovies to deeper zones  
456 during El Niño <sup>75</sup> could lead to higher foraging specialisation of the two seabird species due to  
457 higher competition for prey, as documented in other booby species <sup>84</sup>. Therefore, we would  
458 expect that significant changes in the diet of seabirds could lead to high inter-species differences  
459 in  $\delta^{15}\text{N}$  values during years of less prey abundance, but we did not observe this trend during  
460 our studied period. A pronounced baseline shift in  $\delta^{15}\text{N}$  translated into the local food chain,  
461 caused by a change in nutrient regimes related to the upwelling dynamics driven by ENSO <sup>76</sup> is  
462 most likely the driving factor. Indeed, despite  $\delta^{15}\text{N}$  represents a unique proxy to document  
463 trophic interactions and seabird diet in most ecosystems, the singularity of the upwelling regime  
464 on the N cycle operating at the baseline level of the NHCS is known to induce significant  $\delta^{15}\text{N}$   
465 baseline shifts translated up to marine predators <sup>46,47</sup>. This finding is consistent with (i) field  
466 observations confirming that anchovy was almost the sole species observed in seabird  
467 regurgitates for all years, (ii) that the biomass of anchovies has decreased and stayed low as  
468 soon as 2012 (**Figure 2F**), not influencing the  $\delta^{15}\text{N}$  shift in seabirds during the same period of

469 time, and (iii) that the interannual differences in  $\delta^{13}\text{C}$  and  $\delta^{15}\text{N}$  in the two seabird species reflect  
470 those in anchovies for the same years (Figure S4). Baseline processes are thus mostly  
471 responsible for the interannual differences in  $\delta^{15}\text{N}$  values in seabird blood.

472 Marine oxygen consumption strongly determines N-loss processes, such as  
473 denitrification and anammox<sup>85</sup>, that induce significant N isotopic fractionation. Anaerobic  
474 bacteria use nitrate ( $\text{NO}_3^-$ ) as an oxidant for the degradation of organic matter and its reduction  
475 produces isotopically light products ( $\text{N}_2$  and  $\text{N}_2\text{O}$ ) and isotopically heavier residual nitrate<sup>86,87</sup>.  
476 Also, anaerobic ammonia ( $\text{NH}_4^+$ ) oxidation (anammox) is likely the predominant pathway for  
477 N loss in oceanic OMZs<sup>88</sup>. Both heterotrophic denitrification and anammox processes appear  
478 to decrease significantly under El Niño conditions<sup>89</sup>, coupled to low primary productivity, the  
479 deepening of the OMZ distribution and high bottom water oxygenation. Therefore, lower  
480 organic matter mineralization and limited nitrate supply to surface waters under El Niño  
481 conditions depletes isotopically the particulate organic matter utilized by phytoplankton,  
482 leading to lower  $\delta^{15}\text{N}$  values in biota<sup>89,90</sup>. Consequently, the significant interannual variations  
483 of seabird  $\delta^{15}\text{N}$  are more likely related to shifts in the N isotopic baseline and therefore can be  
484 used as a proxy of oxygenation events/organic matter remineralization, like El Niño or the warm  
485 ENSO events of the NHCS<sup>91</sup>.

### 486 3.5 ENSO driven variability in Hg isotopes

487 Despite the absence of substantial changes in Hg concentration in biota over the studied period,  
488 we detected an enhanced interannual variability of seabird Hg isotopes (Figure 4C-D). We  
489 observed no linear relationship of  $\delta^{202}\text{Hg}$  with ENSO events proxied by ICEN index ( $p=0.08$ )  
490 and no significant  $\delta^{202}\text{Hg}$  interannual variations neither for cormorants (Kruskal Wallis,  
491  $H=17.1$ ,  $p=0.004$ ) nor boobies ( $H=16.4$ ,  $p=0.006$ ). The GAM applied for  $\delta^{202}\text{Hg}$  showed that  
492 the best explanatory variables are  $\delta^{15}\text{N}$ , upwelling index and NPP together, but only explained  
493 for 36 to 40% of the total  $\delta^{202}\text{Hg}$  variability, depending on the integrated area (Table S2).

494 Interannual variability of  $\Delta^{199}\text{Hg}$  of Guanay cormorants and Peruvian boobies was significant  
495 (Kruskal Wallis,  $H=28.8$  and  $32.21$  respectively, both  $p<0.0001$ ) and lower  $\Delta^{199}\text{Hg}$  values were  
496 observed during El Niño years relative to La Niña and normal years for both species ( $H=24.02$ ,  
497  $p<0.0001$ ) (Figure 4D). Both Guanay cormorants and Peruvian boobies exhibited higher  $\Delta^{199}\text{Hg}$   
498 values in 2013 ( $2.57 \pm 0.02$  and  $2.48 \pm 0.05\%$ ), with a pronounced significant decrease in 2015  
499 (boobies:  $1.87 \pm 0.02\%$ ) and 2016 (cormorants:  $1.85 \pm 0.02$  and boobies:  $1.82 \pm 0.08\%$ ).  
500 Significant linear relationships were found between  $\Delta^{199}\text{Hg}$  and  $\delta^{15}\text{N}$  values of cormorants  
501 ( $R^2=0.59$ ,  $p<0.001$ ) and boobies ( $R^2=0.77$ ,  $p<0.001$ ), suggesting that both isotopic signatures  
502 are biogeochemically related and that interannual variations in  $\Delta^{199}\text{Hg}$  and  $\delta^{15}\text{N}$  values are not  
503 trophic or ecologically driven. Additionally, results of GAM showed that seabird  $\Delta^{199}\text{Hg}$  are  
504 strongly explained by oxycline depth, SST and NPP, explaining for 77% of the  $\Delta^{199}\text{Hg}$   
505 interannual variability (Table S2).

506 Due to the sensitivity of  $\Delta^{199}\text{Hg}$  to sea-surface MeHg photochemical reactions, these  
507 results suggest that seabird  $\Delta^{199}\text{Hg}$  values likely reflect the change at which MeHg is formed  
508 and photodegraded, mirroring the oxycline depth oscillations during ENSO events. Indeed, the  
509 sharp decrease of seabird  $\Delta^{199}\text{Hg}$  values during the El Niño 2015-2016 (down to  $\sim 1.8\%$ ) is  
510 coincident with a deepening of the oxycline from 30-50 m to 100 m depth (Figure 2D), and  
511 therefore likely reflects a larger contribution of deeper and less photodegraded MeHg  
512 production. Oxycline depth variability has a direct impact on the biogeochemical processes of  
513 the northern region of the NHCS because oxygen is a control factor in the distribution of many  
514 organisms<sup>53,92</sup>. The bottom depth of the oxycline is the zone where the most intense particulate  
515 organic matter remineralization occurs, an essential process for the maintenance of the Peru  
516 OMZ<sup>93</sup> and Hg methylation. Vertical profiles across a large coastal-oceanic section off Peru  
517 have shown maxima of MeHg concentrations within the OMZ and near the subsurface  
518 chlorophyll maximum<sup>25</sup>, that are expected to be driven by *in situ* microbial methylation in these



519 coastal productive areas. During El Niño episodes, the deepening of the oxycline can favour  
520 the expansion of the vertical habitat of most marine organisms into deeper zones of the water  
521 column that are less connected to the photic zone. In contrast, the sudden increase of seabird  
522  $\Delta^{199}\text{Hg}$  values from 2012 to 2013 is coincident with an increase of  $\delta^{15}\text{N}$  values, and of shallower  
523 oxycline (Figure 2D), likely favouring MeHg formation and photodegradation near the surface  
524 in 2013 in the context of a compressed habitat for anchovy schools.

525 Our results showing profound changes in the depth at which MeHg is formed and  
526 photodegraded while displaying a limited impact on seabird MeHg concentrations during  
527 ENSO can be explained by different factors. We consider two potential explanations for this.  
528 First, photochemical MeHg degradation may not be the dominant MeHg loss mechanism above  
529 the oxycline, leading to measurable ENSO driven  $\Delta^{199}\text{Hg}$  variability but not food web MeHg  
530 variability. Second, photochemical MeHg degradation is the dominant loss mechanism,  
531 enhanced in 2013 due to the shallow oxycline. MeHg photodemethylation is balanced by  
532 enhanced inorganic Hg methylation in the OMZ due to higher primary productivity and ensuing  
533 particle remineralization and Hg methylation in the OMZ under these conditions (Figure 5).  
534 During El Niño events, the deepening of the oxycline leading to reduced MeHg  
535 photodegradation, as suggested by the drop in  $\Delta^{199}\text{Hg}$ , is associated with lower vertical inputs  
536 of organic matter and remineralization traced by lower  $\delta^{15}\text{N}$ , leading to lower MeHg formation.  
537 Finally, we considered the possibility that during La Niña years, a higher advection of nutrients  
538 and organic matter towards the surface increases the supply of MeHg produced at depth (with  
539 close-to zero  $\Delta^{199}\text{Hg}$  values). However, this scenario would lead to a dilution of the highly  
540 photodemethylated MeHg in the surface with MeHg from deeper zones, lowering the  $\Delta^{199}\text{Hg}$   
541 values of MeHg assimilated by biota during La Niña, which is the opposite to our observations.  
542 Consequently, our results reveal that variability in  $\Delta^{199}\text{Hg}$  values of the Peruvian food web are

543 mostly driven by changes in productivity and in oxycline depth rather than water mass mixing,  
544 and that most bioavailable MeHg is produced in the oxycline.

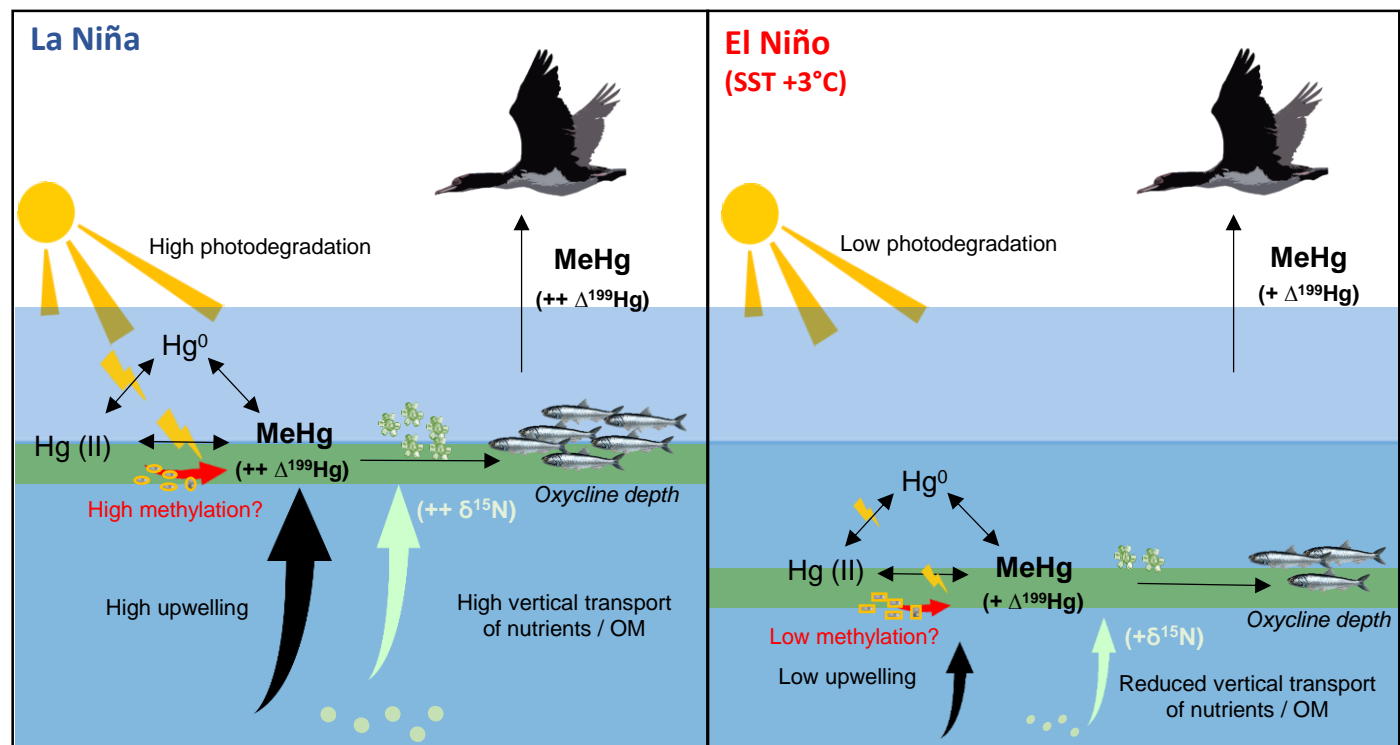
545 In summary, the strong ENSO climate variability of SST, NPP and oxycline depth in  
546 the NHCS and OMZ was not accompanied by variability in marine food web top predator  
547 MeHg concentrations. These observations contrast with recent model predictions, based on  
548 Atlantic Ocean food web data, that ocean warming and overfishing have led to increases in fish  
549 MeHg levels <sup>9</sup>. We suggest that marine MeHg dynamics, food web uptake and bioaccumulation  
550 are more resilient to climate warming than suggested by the model developed in Schartup et al.  
551 2019 <sup>9</sup>. Further research investigating other oceanic regions, and exploring different marine  
552 ecosystems are needed.

553

554

555

556



557

558 **Figure 5. Schematic figure about the dominant Hg processes during contrasted ENSO events. During La Niña (left panel), the conditions of higher supply of nutrient**  
 559 **may favour productivity potentially enhancing in situ microbial methylation/demethylation of Hg in the OMZ. However, since the oxycline is shallower, the extent of**  
 560 **MeHg photodemethylation would be high (leading to higher Δ<sup>199</sup>Hg values). Conversely, during El Niño, lower nutrient supply and remineralization may reduce**  
 561 **microbial Hg methylation rates, and, as the oxycline is much deeper, MeHg photodegradation processes would be inhibited. Both processes (MeHg formation and**  
 562 **MeHg degradation) seem to be compensated, leading to stable MeHg concentrations in the Peruvian food web during extreme ENSO events.**

563

564

#### 565 **4 Acknowledgements**

566 This work was supported by the cooperative agreement between the Institut de Recherche pour  
567 le Développement (IRD), the Peruvian Sea Institute (IMARPE), the Agence Nationale de la  
568 Recherche (ANR) project ‘Top Predators as Indicators of Exploited Marine Ecosystem  
569 dynamics’ (TOPINEME, PI SB), and the International Joint Laboratory DISCOH 1&2 for  
570 sample collection, and funding for carbon and nitrogen isotope and mercury concentration  
571 analysis. We thank Gaël Guillou for carbon and nitrogen stable isotope analysis. We thank the  
572 French National Research Agency ANR-17-CE34-0010 project ‘Unraveling the origin of  
573 methylMERCURY TOXin in marine ecosystems’ (MERTOX, PI DP) for providing financial  
574 support for Hg stable isotopes analysis and for the postdoctoral grant provided to Marina  
575 Renedo.

#### 576 **5 Supporting information paragraph**

577 Further experimental details of methodological approach; Statistical results of generalized  
578 additive models (GAM) models; Detailed QA/QC of Hg isotopic analyses; Complete tables of  
579 Hg concentrations and C, N and Hg isotopic results of seabirds; Supplementary figures: Figure  
580 S1, Spatial resolution of the areas integrated for satellite data; Figure S2, Results of the optimal  
581 GAM models; Figure S3, Interannual variations of 2-month averages of additional physical and  
582 biogeochemical/biological parameters in the NHCS; Figure S4, Annually averaged  $\delta^{15}\text{N}$  and  
583  $\delta^{13}\text{C}$  values of blood samples of seabirds and prey; Figure S5,  $\Delta^{199}\text{Hg}$  *versus*  $\Delta^{201}\text{Hg}$  values of  
584 seabirds and anchovies; Figure S6, Temporal trend of Hg concentrations of anchovy samples  
585 Figure S7, Hg concentrations *versus*  $\delta^{202}\text{Hg}$  values of blood samples of seabirds and anchovies.

586

- 588 (1) Tan, S. W.; Meiller, J. C.; Mahaffey, K. R. The Endocrine Effects of Mercury in Humans  
589 and Wildlife. *Crit. Rev. Toxicol.* **2009**, *39* (3), 228–269.  
590 <https://doi.org/10.1080/10408440802233259>.
- 591 (2) Li, C.; Sonke, J. E.; Le Roux, G.; Piotrowska, N.; Van Der Putten, N.; Roberts, S. J.;  
592 Daley, T.; Rice, E.; Gehrels, R.; Enrico, M.; Mauquoy, D.; Roland, T. P.; De  
593 Vleeschouwer, F. Unequal Anthropogenic Enrichment of Mercury in Earth's Northern  
594 and Southern Hemispheres. *ACS Earth Space Chem.* **2020**, *4* (11), 2073–2081.  
595 <https://doi.org/10.1021/acsearthspacechem.0c00220>.
- 596 (3) Outridge, P. M.; Stern, G. A.; Hamilton, P. B.; Sanei, H. Algal Scavenging of Mercury  
597 in Preindustrial Arctic Lakes. *Limnol. Oceanogr.* **2019**, *64* (4), 1558–1571.  
598 <https://doi.org/10.1002/lno.11135>.
- 599 (4) Kirk, J.; St. Louis, V. L.; Hintelmann, H.; Lehnher, I.; Else, B.; Poissant, L. Methylated  
600 Mercury Species in Marine Waters of the Canadian High and Sub Arctic. *Env. Sci*  
601 *Technol* **2008**, *42* (22), 8367–8373. <https://doi.org/10.1021/es801635m>.
- 602 (5) Monperrus, M.; Tessier, E.; Amouroux, D.; Leynaert, A.; Huonnic, P.; Donard, O. F. X.  
603 Mercury Methylation, Demethylation and Reduction Rates in Coastal and Marine  
604 Surface Waters of the Mediterranean Sea. *Mar. Chem.* **2007**, *107* (1), 49–63.  
605 <https://doi.org/10.1016/j.marchem.2007.01.018>.
- 606 (6) Sunderland, E. M.; Krabbenhoft, D. P.; Moreau, J. W.; Strode, S. A.; Landing, W. M.  
607 Mercury Sources, Distribution, and Bioavailability in the North Pacific Ocean: Insights  
608 from Data and Models. *Glob. Biogeochem. Cycles* **2009**, *23* (2), 1–14.  
609 <https://doi.org/10.1029/2008GB003425>.
- 610 (7) Choy, C. A.; Popp, B. N.; Kaneko, J. J.; Drazen, J. C. The Influence of Depth on Mercury  
611 Levels in Pelagic Fishes and Their Prey. *Proc. Natl. Acad. Sci. U. S. A.* **2009**, *106* (33),  
612 13865–13869.
- 613 (8) Streets, D. G.; Horowitz, H. M.; Lu, Z.; Levin, L.; Thackray, C. P.; Sunderland, E. M.  
614 Global and Regional Trends in Mercury Emissions and Concentrations, 2010–2015.  
615 *Atmos. Environ.* **2019**, *201* (December 2018), 417–427.  
616 <https://doi.org/10.1016/j.atmosenv.2018.12.031>.
- 617 (9) Schartup, A. T.; Thackray, C. P.; Qureshi, A.; Dassuncao, C.; Gillespie, K.; Hanke, A.;  
618 Sunderland, E. M. Climate Change and Overfishing Increase Neurotoxicant in Marine  
619 Predators. *Nature* **2019**, *572* (7771), 648–650. [https://doi.org/10.1038/s41586-019-1468-](https://doi.org/10.1038/s41586-019-1468-9)  
620 [9](https://doi.org/10.1038/s41586-019-1468-9).
- 621 (10) Krabbenhoft, D. P.; Sunderland, E. M. Global Change and Mercury. *Science* **2013**, *341*  
622 (6153), 1457–1458. <https://doi.org/10.1126/science.1242838>.
- 623 (11) IPCC Working Group I, I.; Stocker, T. F.; Qin, D.; Plattner, G.-K.; Tignor, M.; Allen, S.  
624 K.; Boschung, J.; Nauels, A.; Xia, Y.; Bex, V.; Midgley, P. M. IPCC, 2013: Climate  
625 Change 2013: The Physical Science Basis. Contribution of Working Group I to the Fifth  
626 Assessment Report of the Intergovernmental Panel on Climate Change. *Ippc* **2013**, *AR5*  
627 (September 2014), 1535.
- 628 (12) Bindoff, N. L.; Cheung, W. W. L.; Kairo, J. G.; Aristegui, J.; Gunder, V. A.; Hallberg,  
629 R.; Hilmi, N.; Jiao, N.; Karim, M. S.; Levin, L.; O'Donoghue, S.; Purca Cuicapusa, S.  
630 R.; Rinkevich, B.; Suga, T.; Tagliabue, A.; Williamson, P. Changing Ocean, Marine  
631 Ecosystems, and Dependent Communities. *IPCC Spec. Rep. Ocean Cryosphere Chang.*  
632 *Clim.* **2019**, 447–588.
- 633 (13) Gregg, W. W.; Conkright, M. E.; Ginoux, P.; O'Reilly, J. E.; Casey, N. W. Ocean  
634 Primary Production and Climate: Global Decadal Changes. *Geophys. Res. Lett.* **2003**, *30*  
635 (15), 10–13. <https://doi.org/10.1029/2003GL016889>.

- 636 (14) Stramma, L.; Jonhson, G. C.; Sprintall, J.; Mohrholz, V. Expanding Oxygen-Minimum  
637 Zones in the Tropical Oceans. *Science* **2008**, *320*, 655–659.
- 638 (15) Diaz, R. J.; Rosenberg, R. Spreading Dead Zones and Consequences for Marine  
639 Ecosystems. *Science* **2008**, *321* (5891), 926–929.  
640 <https://doi.org/10.1126/science.1156401>.
- 641 (16) Cheung, W. Explaining Ocean Warming: Causes, Scale, Effects and Consequences.  
642 *Explain. Ocean Warm. Causes Scale Eff. Consequences* **2016**, No. January.  
643 <https://doi.org/10.2305/iucn.ch.2016.08.en>.
- 644 (17) Blanchard, J. L.; Jennings, S.; Holmes, R.; Harle, J.; Merino, G.; Allen, J. I.; Holt, J.;  
645 Dulvy, N. K.; Barange, M. Potential Consequences of Climate Change for Primary  
646 Production and Fish Production in Large Marine Ecosystems. *Philos. Trans. R. Soc. B*  
647 *Biol. Sci.* **2012**, *367* (1605), 2979–2989. <https://doi.org/10.1098/rstb.2012.0231>.
- 648 (18) Mason, R. P.; Choi, A. L.; Fitzgerald, W. F.; Hammerschmidt, C. R.; Lamborg, C. H.;  
649 Soerensen, A. L.; Sunderland, E. M. Mercury Biogeochemical Cycling in the Ocean and  
650 Policy Implications. *Environ. Res.* **2012**, *119*, 101–117.  
651 <https://doi.org/10.1016/j.envres.2012.03.013>.
- 652 (19) Dijkstra, J. A.; Buckman, K. L.; Ward, D.; Evans, D. W.; Dionne, M.; Chen, C. Y.  
653 Experimental and Natural Warming Elevates Mercury Concentrations in Estuarine Fish.  
654 *PLoS ONE* **2013**, *8* (3), 1–9. <https://doi.org/10.1371/journal.pone.0058401>.
- 655 (20) Maulvault, A. L.; Custódio, A.; Anacleto, P.; Repolho, T.; Pousão, P.; Nunes, M. L.;  
656 Diniz, M.; Rosa, R.; Marques, A. Bioaccumulation and Elimination of Mercury in  
657 Juvenile Seabass (*Dicentrarchus Labrax*) in a Warmer Environment. *Environ. Res.* **2016**,  
658 *149*, 77–85. <https://doi.org/10.1016/j.envres.2016.04.035>.
- 659 (21) Espinoza-Morriberon, D.; Echevin, V.; Colas, F.; Tam, J.; Ledesma, J.; Vasquez, L.;  
660 Graco, M. Impacts of El Niño Events on the Peruvian Upwelling System Productivity. *J.*  
661 *Geophys. Res. Oceans* **2017**, *122* (7), 5423–5444.  
662 <https://doi.org/10.1002/2016JC012335>.Received.
- 663 (22) Graco, M. I.; Purca, S.; Dewitte, B.; Castro, C. G.; Morón, O.; Ledesma, J.; Flores, G.;  
664 Gutiérrez, D. The OMZ and Nutrient Features as a Signature of Interannual and Low-  
665 Frequency Variability in the Peruvian Upwelling System. *Biogeosciences* **2017**, *14* (20),  
666 4601–4617. <https://doi.org/10.5194/bg-14-4601-2017>.
- 667 (23) Chavez, F. P.; Bertrand, A.; Guevara-Carrasco, R.; Soler, P.; Csirke, J. The Northern  
668 Humboldt Current System: Brief History, Present Status and a View towards the Future.  
669 *Prog. Oceanogr.* **2008**, *79* (2–4), 95–105. <https://doi.org/10.1016/j.pocean.2008.10.012>.
- 670 (24) Gutiérrez, D.; Enríquez, E.; Purca, S.; Quipúzcoa, L.; Marquina, R.; Flores, G.; Graco,  
671 M. Oxygenation Episodes on the Continental Shelf of Central Peru: Remote Forcing and  
672 Benthic Ecosystem Response. *Prog. Oceanogr.* **2008**, *79* (2–4), 177–189.  
673 <https://doi.org/10.1016/j.pocean.2008.10.025>.
- 674 (25) Bowman, K. L.; Hammerschmidt, C. R.; Lamborg, C. H.; Swarr, G. J.; Agather, A. M.  
675 Distribution of Mercury Species across a Zonal Section of the Eastern Tropical South  
676 Pacific Ocean (U.S. GEOTRACES GP16). *Mar. Chem.* **2016**, *186*, 156–166.  
677 <https://doi.org/10.1016/j.marchem.2016.09.005>.
- 678 (26) Bowman, K. L.; Lamborg, C. H.; Agather, A. M. A Global Perspective on Mercury  
679 Cycling in the Ocean. *Sci. Total Environ.* **2020**, *710*, 136166.  
680 <https://doi.org/10.1016/j.scitotenv.2019.136166>.
- 681 (27) Apaza, M.; Figari, A. Mortandad de Aves Marinas Durante “El Niño 1997-98” En El  
682 Litoral Sur de San Juan de Marcona, ICA -Perú. *Rev. Peru. Biol.* **1999**, *6* (3), 110–117.  
683 <https://doi.org/10.15381/rpb.v6i3.8436>.

- 684 (28) Ñiquen, M.; Bouchon, M. Impact of El Niño Events on Pelagic Fisheries in Peruvian  
685 Waters. *Deep-Sea Res. Part II Top. Stud. Oceanogr.* **2004**, *51* (6–9), 563–574.  
686 <https://doi.org/10.1016/j.dsr2.2004.03.001>.
- 687 (29) Bertrand, A.; Lengaigne, M.; Takahashi, K.; Avadi, A.; Poulain, F.; Harrod, C. *El Niño*  
688 *Southern Oscillation (ENSO) Effects on Fisheries and Aquaculture*; 2020.  
689 <https://doi.org/10.4060/ca8348en>.
- 690 (30) Zavalaga, C. B.; Paredes, R. Foraging Behaviour and Diet of the Guanay Cormorant.  
691 *South Afr. J. Mar. Sci.* **1999**, No. 21, 251–258.  
692 <https://doi.org/10.2989/025776199784125980>.
- 693 (31) Weimerskirch, H.; Bertrand, S.; Silva, J.; Bost, C.; Peraltilla, S. Foraging in Guanay  
694 Cormorant and Peruvian Booby, the Major Guano-Producing Seabirds in the Humboldt  
695 Current System. *Mar. Ecol. Prog. Ser.* **2012**, *458*, 231–245.  
696 <https://doi.org/10.3354/meps09752>.
- 697 (32) Carravieri, A.; Bustamante, P.; Tartu, S.; Meillère, A.; Labadie, P.; Budzinski, H.;  
698 Peluhet, L.; Barbraud, C.; Weimerskirch, H.; Chastel, O.; Cherel, Y. Wandering  
699 Albatrosses Document Latitudinal Variations in the Transfer of Persistent Organic  
700 Pollutants and Mercury to Southern Ocean Predators. *Environ. Sci. Technol.* **2014**, *48*  
701 (24), 14746–14755. <https://doi.org/10.1021/es504601m>.
- 702 (33) Albert, C.; Renedo, M.; Bustamante, P.; Fort, J. Using Blood and Feathers to Investigate  
703 Large-Scale Hg Contamination in Arctic Seabirds: A Review. *Environ. Res.* **2019**, *177*.  
704 <https://doi.org/10.1016/j.envres.2019.108588>.
- 705 (34) Renedo, M.; Amouroux, D.; Duval, B.; Carravieri, A.; Tessier, E.; Barre, J.; Bérail, S.;  
706 Pedrero, Z.; Cherel, Y.; Bustamante, P. Seabird Tissues As Efficient Biomonitoring  
707 Tools for Hg Isotopic Investigations: Implications of Using Blood and Feathers from  
708 Chicks and Adults. *Environ. Sci. Technol.* **2018**, *52* (7), 4227–4234.  
709 <https://doi.org/10.1021/acs.est.8b00422>.
- 710 (35) Bearhop, S.; Ruxton, G. D.; Furness, R. W. Dynamics of Mercury in Blood and Feathers  
711 of Great Skuas. *Environ. Toxicol. Chem.* **2000**, *19* (6), 1638–1643.  
712 [https://doi.org/10.1897/1551-5028\(2000\)019<1638:Domiba>2.3.Co;2](https://doi.org/10.1897/1551-5028(2000)019<1638:Domiba>2.3.Co;2).
- 713 (36) Renedo, M.; Amouroux, D.; Pedrero, Z.; Bustamante, P.; Cherel, Y. Identification of  
714 Sources and Bioaccumulation Pathways of MeHg in Subantarctic Penguins : A Stable  
715 Isotopic Investigation. *Sci. Rep.* **2018**, *8* (8865). [https://doi.org/10.1038/s41598-018-](https://doi.org/10.1038/s41598-018-27079-9)  
716 [27079-9](https://doi.org/10.1038/s41598-018-27079-9).
- 717 (37) Renedo, M.; Bustamante, P.; Cherel, Y.; Pedrero, Z.; Tessier, E.; Amouroux, D. A  
718 “Seabird-Eye” on Mercury Stable Isotopes and Cycling in the Southern Ocean. *Sci. Total*  
719 *Environ.* **2020**, *742*, 140499. <https://doi.org/10.1016/j.scitotenv.2020.140499>.
- 720 (38) Blum, J. D.; Popp, B. N.; Drazen, J. C.; Anela Choy, C.; Johnson, M. W. Methylmercury  
721 Production below the Mixed Layer in the North Pacific Ocean. *Nat. Geosci.* **2013**, *6* (10),  
722 879–884. <https://doi.org/10.1038/ngeo1918>.
- 723 (39) Li, M.; Juang, C. A.; Ewald, J. D.; Yin, R.; Mikkelsen, B.; Krabbenhoft, D. P.; Balcom,  
724 P. H.; Dassuncao, C.; Sunderland, E. M. Selenium and Stable Mercury Isotopes Provide  
725 New Insights into Mercury Toxicokinetics in Pilot Whales. *Sci. Total Environ.* **2020**,  
726 *710*, 136325. <https://doi.org/10.1016/j.scitotenv.2019.136325>.
- 727 (40) Bergquist, B. A.; Blum, J. D. Mass-Dependent and -Independent Fractionation of Hg  
728 Isotopes by Photoreduction in Aquatic Systems. *Science* **2007**, *318* (5849), 417–420.  
729 <https://doi.org/10.1126/science.1148050>.
- 730 (41) Zheng, W.; Foucher, D.; Hintelmann, H. Mercury Isotope Fractionation during  
731 Volatilization of Hg(0) from Solution into the Gas Phase. *J. Anal. At. Spectrom.* **2007**,  
732 *22* (9), 1097. <https://doi.org/10.1039/b705677j>.

- 733 (42) Le Croizier, G.; Lorrain, A.; Sonke, J. E.; Jaquemet, S.; Schaal, G.; Renedo, M.; Besnard,  
734 L.; Cherel, Y.; Point, D. Mercury Isotopes as Tracers of Ecology and Metabolism in Two  
735 Sympatric Shark Species. *Environ. Pollut.* **2020**, No. June, 114931.  
736 <https://doi.org/10.1016/j.envpol.2020.114931>.
- 737 (43) Perrot, V.; Masbou, J.; Pastukhov, M. V.; Epov, V. N.; Point, D.; Bérail, S.; Becker, P.  
738 R.; Sonke, J. E.; Amouroux, D. Natural Hg Isotopic Composition of Different Hg  
739 Compounds in Mammal Tissues as a Proxy for in Vivo Breakdown of Toxic  
740 Methylmercury. *Metallomics* **2016**, 8 (2), 170–178.  
741 <https://doi.org/10.1039/C5MT00286A>.
- 742 (44) Janssen, S. E.; Schaefer, J. K.; Barkay, T.; Reinfelder, J. R. Fractionation of Mercury  
743 Stable Isotopes during Microbial Methylmercury Production by Iron- and Sulfate-  
744 Reducing Bacteria. *Environ. Sci. Technol.* **2016**, 50 (15), 8077–8083.  
745 <https://doi.org/10.1021/acs.est.6b00854>.
- 746 (45) Kwon, S. Y.; Blum, J. D.; Carvan, M. J.; Basu, N.; Head, J. A.; Madenjian, C. P.; David,  
747 S. R. Absence of Fractionation of Mercury Isotopes during Trophic Transfer of  
748 Methylmercury to Freshwater Fish in Captivity. *Environ. Sci. Technol.* **2012**, 46 (14),  
749 7527–7534. <https://doi.org/10.1021/es300794q>.
- 750 (46) Espinoza, P.; Lorrain, A.; Ménard, F.; Cherel, Y.; Tremblay-Boyer, L.; Argüelles, J.;  
751 Tafur, R.; Bertrand, S.; Tremblay, Y.; Ayón, P.; Munaron, J. M.; Richard, P.; Bertrand,  
752 A. Trophic Structure in the Northern Humboldt Current System: New Perspectives from  
753 Stable Isotope Analysis. *Mar. Biol.* **2017**, 164 (4), 0. <https://doi.org/10.1007/s00227-017-3119-8>.
- 754 (47) Argüelles, J.; Lorrain, A.; Cherel, Y.; Graco, M.; Tafur, R.; Alegre, A.; Espinoza, P.;  
755 Taipe, A.; Ayón, P.; Bertrand, A. Tracking Habitat and Resource Use for the Jumbo  
756 Squid *Dosidicus Gigas*: A Stable Isotope Analysis in the Northern Humboldt Current  
757 System. *Mar. Biol.* **2012**, 159 (9), 2105–2116. <https://doi.org/10.1007/s00227-012-1998-2>.
- 758 (48) Post, D. M. Using Stable Isotopes to Estimate Trophic Position: Models, Methods, and  
759 Assumptions. *Ecology* **2002**, 83 (3), 703–718. [https://doi.org/10.1890/0012-9658\(2002\)083\[0703:USITET\]2.0.CO;2](https://doi.org/10.1890/0012-9658(2002)083[0703:USITET]2.0.CO;2).
- 760 (49) Cherel, Y.; Hobson, K. A. Geographical Variation in Carbon Stable Isotope Signatures  
761 of Marine Predators : A Tool to Investigate Their Foraging Areas in the Southern Ocean.  
762 *Mar. Ecol. Prog. Ser.* **2007**, 329, 281–287.
- 763 (50) Bertrand, S.; Díaz, E.; Lengaigne, M. Patterns in the Spatial Distribution of Peruvian  
764 Anchovy (*Engraulis Ringens*) Revealed by Spatially Explicit Fishing Data. *Prog.*  
765 *Oceanogr.* **2008**, 79 (2–4), 379–389. <https://doi.org/10.1016/j.pocean.2008.10.009>.
- 766 (51) Gutiérrez, M.; Swartzman, G.; Bertrand, A.; Bertrand, S. Anchovy (*Engraulis Ringens*)  
767 and Sardine (*Sardinops Sagax*) Spatial Dynamics and Aggregation Patterns in the  
768 Humboldt Current Ecosystem, Peru, from 1983-2003. *Fish. Oceanogr.* **2007**, 16 (2),  
769 155–168. <https://doi.org/10.1111/j.1365-2419.2006.00422.x>.
- 770 (52) Gutiérrez, M.; Castillo, R.; Segura, M.; Peraltilla, S.; Flores, M. Trends in Spatio-  
771 Temporal Distribution of Peruvian Anchovy and Other Small Pelagic Fish Biomass from  
772 1966-2009. *Lat. Am. J. Aquat. Res.* **2012**, 40 (3 SPL. ISS.), 633–648.  
773 <https://doi.org/10.3856/vol40-issue3-fulltext-12>.
- 774 (53) Bertrand, A.; Ballón, M.; Chaigneau, A. Acoustic Observation of Living Organisms  
775 Reveals the Upper Limit of the Oxygen Minimum Zone. *PLoS ONE* **2010**, 5 (4).  
776 <https://doi.org/10.1371/journal.pone.0010330>.
- 777 (54) Espinoza-morriberón, D.; Echevin, V.; Colas, F.; Tam, J. Oxygen Variability During  
778 ENSO in the Tropical South Eastern Pacific. **2019**, No. January.  
779 <https://doi.org/10.3389/fmars.2018.00526>.
- 780  
781  
782



- 783 (55) Simmonds, E. J.; Gutiérrez, M.; Chipollini, A.; Gerlotto, F.; Woillez, M.; Bertrand, A.  
784 Optimizing the Design of Acoustic Surveys of Peruvian Anchoveta. *ICES J. Mar. Sci.*  
785 **2009**, *66* (6), 1341–1348. <https://doi.org/10.1093/icesjms/fsp118>.
- 786 (56) Food and Agriculture Organization of the United Nations (FAO) [www.fao.org/](http://www.fao.org/publications)  
787 publications.
- 788 (57) Anuario Estadístico Pesquero y Acuícola, Ministerio de Produccion del Perú  
789 [https://ogeiee.produce.gob.pe/index.php/en/oe-documentos-](https://ogeiee.produce.gob.pe/index.php/en/oe-documentos-publicaciones/publicaciones-anauales?start=0)  
790 [publicaciones/publicaciones-anauales?start=0](https://ogeiee.produce.gob.pe/index.php/en/oe-documentos-publicaciones/publicaciones-anauales?start=0).
- 791 (58) Takahashi, K.; Mosquera, K.; Reupo, J. El Índice Costero El Niño (ICEN): Historia y  
792 Actualización. *Bol. Téc. Gener. Model. Climáticos Para El Pronóstico Ocurr. Fenóm.*  
793 *El Niño* **2014**, *1*, 2–4.
- 794 (59) R Core Team, 2016: A Language and Environment for Statistical Computing. R  
795 Foundation for Statistical Computing, Vienna, Austria.
- 796 (60) Burnham, K. P.; Anderson, D. R. Multimodel Inference: Understanding AIC and BIC in  
797 Model Selection. *Sociol. Methods Res.* **2004**, *33* (2), 261–304.  
798 <https://doi.org/10.1177/0049124104268644>.
- 799 (61) Wood, S.; Wood, M. S. *Package “Mgcv”. R Package Version (No. 1.8-28)*.
- 800 (62) Zuur, A. F.; Ieno, E. N.; Walker, N. J.; Saveliev, A. A.; Smith, G. M. Mixed Effects  
801 Models and Extensions in Ecology with R. *J. Stat. Softw.* **2009**, *32* (Book Review 1), 1–  
802 4. <https://doi.org/10.18637/jss.v032.b01>.
- 803 (63) ENFEN. *Definición Operacional de Los Eventos El Niño y La Niña y Sus Magnitudes*  
804 *En La Costa Del Perú*; 2012.
- 805 (64) Dewitte, B.; Vazquez-Cuervo, J.; Goubanova, K.; Illig, S.; Takahashi, K.; Cambon, G.;  
806 Purca, S.; Correa, D.; Gutierrez, D.; Sifeddine, A.; Ortlieb, L. Change in El Niño  
807 Flavours over 1958-2008: Implications for the Long-Term Trend of the Upwelling off  
808 Peru. *Deep-Sea Res. Part II Top. Stud. Oceanogr.* **2012**, *77–80*, 143–156.  
809 <https://doi.org/10.1016/j.dsr2.2012.04.011>.
- 810 (65) Takahashi, K.; Montecinos, A.; Goubanova, K.; Dewitte, B. ENSO Regimes:  
811 Reinterpreting the Canonical and Modoki El Nio. *Geophys. Res. Lett.* **2011**, *38* (10), 1–  
812 5. <https://doi.org/10.1029/2011GL047364>.
- 813 (66) Kessler, W. S. The Circulation of the Eastern Tropical Pacific: A Review. *Prog.*  
814 *Oceanogr.* **2006**, *69* (2–4), 181–217. <https://doi.org/10.1016/j.pocean.2006.03.009>.
- 815 (67) Stramma, L.; Fischer, T.; Grundle, D. S.; Krahnmann, G.; Bange, H. W.; Marandino, C.  
816 A. Observed El Niño Conditions in the Eastern Tropical Pacific in October 2015. *Ocean*  
817 *Sci.* **2016**, *12* (4), 861–873. <https://doi.org/10.5194/os-12-861-2016>.
- 818 (68) Pennington, J. T.; Mahoney, K. L.; Kuwahara, V. S.; Kolber, D. D.; Calienes, R.; Chavez,  
819 F. P. Primary Production in the Eastern Tropical Pacific: A Review. *Prog. Oceanogr.*  
820 **2006**, *69* (2–4), 285–317. <https://doi.org/10.1016/j.pocean.2006.03.012>.
- 821 (69) Lehodey, P.; Bertrand, A.; Hobday, A. J.; Kiyofuji, H.; McClatchie, S.; Menkès, C. E.;  
822 Pilling, G.; Polovina, J.; Tommasi, D. ENSO Impact on Marine Fisheries and  
823 Ecosystems. **2020**, No. November, 429–451.  
824 <https://doi.org/10.1002/9781119548164.ch19>.
- 825 (70) Barbraud, C.; Bertrand, A.; Bouchón, M.; Chaigneau, A.; Delord, K.; Demarcq, H.;  
826 Gimenez, O.; Torero, M. G.; Gutiérrez, D.; Oliveros-Ramos, R.; Passuni, G.; Tremblay,  
827 Y.; Bertrand, S. Density Dependence, Prey Accessibility and Prey Depletion by Fisheries  
828 Drive Peruvian Seabird Population Dynamics. *Ecography* **2018**, *41* (7), 1092–1102.  
829 <https://doi.org/10.1111/ecog.02485>.
- 830 (71) Renedo, M.; Pedrero, Z.; Amouroux, D.; Cherel, Y.; Bustamante, P. Mercury Isotopes  
831 of Key Tissues Document Mercury Metabolic Processes in Seabirds. *Chemosphere* **2021**,  
832 *263*, 127777. <https://doi.org/10.1016/j.chemosphere.2020.127777>.

- 833 (72) Miller, T. W.; Brodeur, R. D.; Rau, G. H. Carbon Stable Isotopes Reveal Relative  
834 Contribution of Shelf-Slope Production to the Northern California Current Pelagic  
835 Community. *Limnol. Oceanogr.* **2008**, *53* (4), 1493–1503.  
836 <https://doi.org/10.4319/lo.2008.53.4.1493>.
- 837 (73) Passuni, G.; Barbraud, C.; Chaigneau, A.; Demarcq, H.; Ledesma, J.; Bertrand, A.;  
838 Castillo, R.; Perea, A.; Mori, J.; Viblanc, V. A.; Torres-Maita, J.; Bertrand, S. Seasonality  
839 in Marine Ecosystems: Peruvian Seabirds, Anchovy, and Oceanographic Conditions.  
840 *Ecology* **2016**, *97* (1), 182–193. <https://doi.org/10.1890/14-1134.1>.
- 841 (74) Lourey, M. J.; Trull, T. W.; Tilbrook, B. Sensitivity of  $\Delta^{13}\text{C}$  of Southern Ocean  
842 Suspended and Sinking Organic Matter to Temperature, Nutrient Utilization, and  
843 Atmospheric  $\text{CO}_2$ . *Deep-Sea Res. Part Oceanogr. Res. Pap.* **2004**, *51* (2), 281–305.  
844 <https://doi.org/10.1016/j.dsr.2003.10.002>.
- 845 (75) Bertrand, A.; Gerlotto, F.; Bertrand, S.; Gutiérrez, M.; Alza, L.; Chipollini, A.; Díaz, E.;  
846 Espinoza, P.; Ledesma, J.; Quesquén, R.; Peraltilla, S.; Chavez, F. Schooling Behaviour  
847 and Environmental Forcing in Relation to Anchoveta Distribution: An Analysis across  
848 Multiple Spatial Scales. *Prog. Oceanogr.* **2008**, *79* (2–4), 264–277.  
849 <https://doi.org/10.1016/j.pocean.2008.10.018>.
- 850 (76) Yang, S.; Gruber, N.; Long, M. C.; Vogt, M. ENSO-Driven Variability of Denitrification  
851 and Suboxia in the Eastern Tropical Pacific Ocean. *Glob. Biogeochem. Cycles* **2017**, *31*  
852 (10), 1470–1487. <https://doi.org/10.1002/2016GB005596>.
- 853 (77) Kritee, K.; Barkay, T.; Blum, J. D. Mass Dependent Stable Isotope Fractionation of  
854 Mercury during Mer Mediated Microbial Degradation of Monomethylmercury.  
855 *Geochim. Cosmochim. Acta* **2009**, *73* (5), 1285–1296.  
856 <https://doi.org/10.1016/j.gca.2008.11.038>.
- 857 (78) Kritee, K.; Blum, J. D.; Barkay, T. Mercury Stable Isotope Fractionation during  
858 Reduction of  $\text{Hg(II)}$  by Different Microbial Pathways. *Environ. Sci. Technol.* **2008**, *42*  
859 (24), 9171–9177. <https://doi.org/10.1021/es801591k>.
- 860 (79) Kwon, S. Y.; Blum, J. D.; Chirby, M. a; Chesney, E. J. Application of Mercury Isotopes  
861 for Tracing Trophic Transfer and Internal Distribution of Mercury in Marine Fish  
862 Feeding Experiments. *Environ. Toxicol. Chem. SETAC* **2013**, *32* (10), 2322–2330.  
863 <https://doi.org/10.1002/etc.2313>.
- 864 (80) Laffont, L.; Sonke, J. E.; Maurice, L.; Hintelmann, H.; Pouilly, M.; Sanchez Bacarreza,  
865 Y.; Perez, T.; Behra, P. Anomalous Mercury Isotopic Compositions of Fish and Human  
866 Hair in the Bolivian Amazon. *Env. Sci Technol* **2009**, *43*, 8985–8990.
- 867 (81) Kwon, S. Y.; Blum, J. D.; Chen, C. Y.; Meattley, D. E.; Mason, R. P. Mercury Isotope  
868 Study of Sources and Exposure Pathways of Methylmercury in Estuarine Food Webs in  
869 the Northeastern U.S. *Env. Sci Technol* **2014**, *48*, 10089–10097.  
870 <https://doi.org/10.1021/es5020554.ome>.
- 871 (82) Zarn, A. M.; Valle, C. A.; Brasso, R.; Fetzner, W. D.; Emslie, S. D. Stable Isotope and  
872 Mercury Analyses of the Galapagos Islands Seabird Community. *Mar. Ornithol.* **2020**,  
873 *48* (1), 71–80.
- 874 (83) Picaut, J.; Hackert, E.; Busalacchi, A. J.; Murtugudde, R.; Picaut J., Hackert E., B. A. J.;  
875 Murtugudde, R.; Lagerloef, G. S. E. Mechanisms of the 1997–1998 El Niño–La Niña, as  
876 Inferred from Space-Based Observations. *J. Geophys. Res.* **2002**, *107* (C5).  
877 <https://doi.org/10.1029/2001jc000850>.
- 878 (84) Ancona, S.; Calixto-Albarrán, I.; Drummond, H. Effect of El Niño on the Diet of a  
879 Specialist Seabird, *Sula Nebouxii*, in the Warm Eastern Tropical Pacific. *Mar. Ecol.*  
880 *Prog. Ser.* **2012**, *462* (May 2014), 261–271. <https://doi.org/10.3354/meps09851>.
- 881 (85) Lam, P.; Lavik, G.; Jensen, M. M.; Van Vossenberg, J. De; Schmid, M.; Woebken, D.;  
882 Gutiérrez, D.; Amann, R.; Jetten, M. S. M.; Kuypers, M. M. M. Revising the Nitrogen

- 883 Cycle in the Peruvian Oxygen Minimum Zone. *Proc. Natl. Acad. Sci. U. S. A.* **2009**, *106*  
884 (12), 4752–4757. <https://doi.org/10.1073/pnas.0812444106>.
- 885 (86) Granger, J.; Sigman, D. M.; Lehmann, M. F.; Tortell, P. D. Nitrogen and Oxygen Isotope  
886 Fractionation during Dissimilatory Nitrate Reduction by Denitrifying Bacteria. *Limnol.*  
887 *Oceanogr.* **2008**, *53* (6), 2533–2545. <https://doi.org/10.4319/lo.2008.53.6.2533>.
- 888 (87) Cline, J. D.; Kaplan, I. R. Isotopic Fractionation of Dissolved Nitrate during  
889 Denitrification in the Eastern Tropical North Pacific Ocean. *Mar. Chem.* **1975**, *3* (1330),  
890 271–299.
- 891 (88) Hamersley, M. R.; Lavik, G.; Woebken, D.; Rattray, J. E.; Lam, P.; Hopmans, E. C.;  
892 Sinninghe Damsté, J. S.; Krüger, S.; Graco, M.; Gutiérrez, D.; Kuypers, M. M. M.  
893 Anaerobic Ammonium Oxidation in the Peruvian Oxygen Minimum Zone. *Limnol.*  
894 *Oceanogr.* **2007**, *52* (3), 923–933. <https://doi.org/10.4319/lo.2007.52.3.0923>.
- 895 (89) Dale, A. W.; Graco, M.; Wallmann, K. Strong and Dynamic Benthic-Pelagic Coupling  
896 and Feedbacks in a Coastal Upwelling System (Peruvian Shelf). *Front. Mar. Sci.* **2017**,  
897 *4* (FEB), 1–17. <https://doi.org/10.3389/fmars.2017.00029>.
- 898 (90) Kock, A.; Arevalo-Martinez, D. L.; Loscher, C. R.; Bange, H. W. Extreme N<sub>2</sub>O  
899 Accumulation in the Coastal Oxygen Minimum Zone off Peru. *Biogeosciences* **2016**, *13*  
900 (3), 827–840. <https://doi.org/10.5194/bg-13-827-2016>.
- 901 (91) Mollier-Vogel, E.; Ryabenko, E.; Martinez, P.; Wallace, D.; Altabet, M. A.; Schneider,  
902 R. Nitrogen Isotope Gradients off Peru and Ecuador Related to Upwelling, Productivity,  
903 Nutrient Uptake and Oxygen Deficiency. *Deep-Sea Res. Part Oceanogr. Res. Pap.* **2012**,  
904 *70*, 14–25. <https://doi.org/10.1016/j.dsr.2012.06.003>.
- 905 (92) Bertrand, A.; Chaigneau, A.; Peraltilla, S.; Ledesma, J.; Graco, M.; Monetti, F.; Chavez,  
906 F. P. Oxygen: A Fundamental Property Regulating Pelagic Ecosystem Structure in the  
907 Coastal Southeastern Tropical Pacific. *PLoS ONE* **2011**, *6* (12), 2–9.  
908 <https://doi.org/10.1371/journal.pone.0029558>.
- 909 (93) Paulmier, A.; Ruiz-Pino, D.; Garçon, V.; Farías, L. Maintaining of the Eastern South  
910 Pacific Oxygen Minimum Zone (OMZ) off Chile. *Geophys. Res. Lett.* **2006**, *33* (20), 2–  
911 7. <https://doi.org/10.1029/2006GL026801>.
- 912